JEM Journal of Experimental Medicine

ARTICLE

TACI regulates marginal zone B cell development

Daisy H. Luff[1], Lesley Vanes[1], Stefan Boeing[1], and Victor L.J. Tybulewicz[1]

The mature B cell compartment consists of follicular and marginal zone (MZ) B cells, which develop from transitional type 2 (T2) B cells. TACI, a member of the TNF receptor superfamily, is expressed on all mature B cells, with highest levels on MZ B cells and plasma cells. Previous studies reported that TACI is a negative regulator of B cell survival. However, this conclusion is confounded by elevated levels of BAFF, a cytokine that supports B cell survival, in TACI-deficient mice. We now show that TACI does not directly regulate B cell survival in mice but rather has a cell-intrinsic role in MZ B cell development. Loss of TACI leads to reduced MZ B cell numbers and an impaired T-independent antibody response. Mechanistically, we show that TACI is required for MZ B cell development from T2 B cell precursors via activation of the PI3K-AKT pathway and subsequent inhibition of the FOXO1 transcription factor.

Introduction

B lymphocyte development is a continuous process in adult mammals, starting in the bone marrow where B cell progenitors undergo immunoglobulin heavy chain and then light chain gene rearrangements (Hardy and Hayakawa, 2001). Successful rearrangement results in the production of immature B cells expressing a diverse repertoire of B cell antigen receptors (BCRs) in the form of surface immunoglobulin M (IgM) associated with CD79A and CD79B signaling subunits. These immature B cells exit the bone marrow and migrate through the blood to the spleen, arriving as transitional type 1 (T1) B cells that mature into T2 B cells and finally into either follicular (FO) or marginal zone (MZ) mature B cells (Pillai and Cariappa, 2009). FO B cells continuously recirculate between the spleen and other lymphoid organs and reside in the follicles of these tissues, where in the presence of cognate T cell help, they generate T-dependent (TD) antibody responses. In contrast, MZ B cells are enriched in the MZ of the spleen where they can rapidly respond to blood-borne antigens and also capture and deliver them to the follicle (Cinamon et al., 2008). The ability of MZ B cells to respond to antigen and differentiate into antibody-secreting cells without cognate T cell help enables them to generate T-independent antibody responses, for example, to repetitive polysaccharide antigens (Martin et al., 2001). A third type of mature B cell, B1 cells, is generated predominantly during fetal and early postnatal stages, has a more limited BCR repertoire, is maintained by self-renewal, and localizes to both lymphoid and nonlymphoid tissues such as the peritoneal and pleural cavities (Hardy, 2006; Vergani et al., 2022).

The development of T2 B cells into mature B cells and the decision whether they become FO or MZ B cells are incompletely understood. It is regulated in part by BCR signaling strength, which is dependent on reactivity of the BCR to self-antigens (Tan et al., 2019). Too little BCR signaling and cells die by neglect, whereas too much autoreactivity and BCR signaling lead to elimination of the B cells by negative selection. In between these two outcomes, T2 B cells are positively selected into mature B cells, with the FO fate being acquired by cells with a broad range of self-reactivity and thus BCR signaling strength, whereas the MZ fate is adopted by B cells with stronger BCR signaling resulting from a higher and narrower range of self-reactivity (Noviski et al., 2019; Wen et al., 2005). In addition to the BCR, MZ B cell development also requires signaling from the NOTCH2 receptor (Pillai and Cariappa, 2009).

The overall size of the FO and MZ B cell pools remains stable in the adult animal (Cancro, 2004). Both FO and MZ B cells are unable to self-renew and are maintained by continuous production of immature B cells in the bone marrow. Homeostasis is determined by a balance between the rate of entry of B cells differentiating from T2 B cells into the mature FO and MZ B cell pools and the rate of exit of cells from these pools because of death or activation-induced differentiation into germinal center B cells, memory B cells, or plasma cells. Thus, the regulation of B cell survival is critical for the maintenance of mature B cell pool sizes.

Two receptors are known to regulate the survival of mature B cells—the BCR and BAFFR (Schweighoffer and Tybulewicz, 2018). Several studies suggest that the BCR delivers a survival signal via the associated CD79A and CD79B proteins and the SYK protein tyrosine kinase (Kraus et al., 2004; Lam et al., 1997; Schweighoffer et al., 2013). Inducible genetic ablation of IgM, CD79A, or SYK results in the loss of all mature B cells (FO, MZ, and B1 cells). This "tonic" BCR survival signal is below the level required for B cell activation and may be dependent on binding to self-antigens. BAFFR, a member of the TNF receptor

[1]The Francis Crick Institute, London, UK.

Correspondence to Victor L.J. Tybulewicz: victor.t@crick.ac.uk; Daisy H. Luff: daisy.luff@crick.ac.uk.

superfamily, is a receptor for the cytokine BAFF. Genetic ablation of either BAFF or BAFFR or antibody-mediated blockade of BAFF-BAFFR binding results in loss of T2 B cells, as well as FO and MZ mature B cells, but not B1 cells (Gross et al., 2000; Gross et al., 2001; Mackay et al., 1999; Mackay et al., 2010; Miller and Hayes, 1991; Rauch et al., 2009; Sasaki et al., 2004; Schiemann et al., 2001; Schneider et al., 2001; Shulga-Morskaya et al., 2004; Smulski and Eibel, 2018; Thompson et al., 2001). Despite the importance of BAFF-BAFFR signaling for B cell survival, the biochemical mechanism by which the receptor delivers survival signals is unclear. The best described signaling pathway from BAFFR involves BAFF-dependent binding of TRAF3 to BAFFR resulting in the activation of IKK1 and the noncanonical NF-κB pathway (Gardam and Brink, 2014). However, inducible deletion of *Ikk1* had no impact on the numbers of mature B cells, demonstrating that this pathway was not required for mature B cell survival (Jellusova et al., 2013). Interestingly, BAFFR has been shown to transduce survival signals in part via BCR, CD19, and SYK, leading to activation of phosphoinositide 3-kinase (PI3K) and ERK pathways (Jellusova et al., 2013; Keppler et al., 2015; Schweighoffer et al., 2013). However, it is not known how BAFFR signals are transduced to these proteins, since TRAF3, the only protein reported to bind to the intracellular domain (ICD) of BAFFR, has not been shown to transduce signals to the BCR, SYK, ERK, or PI3K pathways.

To investigate the mechanism by which BAFFR signals, we used affinity purification (AP) of BAFFR and mass spectrometry to identify new proteins that interact with BAFFR. We show that BAFFR associates with TACI, a related TNF receptor superfamily protein that binds BAFF and the cytokine APRIL. Previous studies had concluded that TACI was a negative regulator of B cell survival, since TACI-deficient mice have expanded numbers of B cells (Shulga-Morskaya et al., 2004; von Bulow et al., 2001; Yan et al., 2001). However, we now demonstrate that TACI does not directly regulate the survival of either FO or MZ B cells. Instead, we show for the first time that TACI deficiency in mice leads to a loss of MZ B cells, owing to a cell-intrinsic function in the development of MZ B cells from T2 B cells. Furthermore, we show that TACI regulates MZ development most likely by transducing signals via PI3K and AKT, leading to inhibition of the FOXO1 transcription factor (TF) and reduced *Klf2* expression. Thus, our study uncovers an unexpected role of TACI and reveals a novel pathway regulating the MZ versus FO cell-fate decision, functioning alongside the BCR and NOTCH2. The work also widens our view of how TNF receptor superfamily members regulate the development and maintenance of the mature B cell repertoire.

Results

Loss of TACI leads to reduced numbers of MZ B cells

To gain a better understanding of how BAFFR transduces signals leading to B cell survival, we generated mice expressing BAFFR with two copies of a Strep-tag II affinity tag at its C terminus (Fig. S1 A). We used AP to isolate BAFFR-Twin-Strep-tag from LPS-activated B cells, which had been untreated or stimulated with BAFF for 15 min, followed by mass spectrometry to identify proteins associated with BAFFR. As expected, we identified BAFFR in all pull-downs and BAFF in pull-downs from stimulated cells. One other protein, the receptor TACI, copurified with BAFFR, and this association only occurred in BAFF-stimulated cells (Fig. S1 B and Table S1). Thus, we hypothesized that TACI may cooperate with BAFFR to regulate B cell survival. In considering this idea, we noted previous publications showing that loss of TACI (encoded by the *Tnfrsf13b* gene) in *Tnfrsf13b*$^{-/-}$ mice results in increased B cell numbers, suggesting that TACI is a negative regulator of B cell survival (Shulga-Morskaya et al., 2004; von Bulow et al., 2001; Yan et al., 2001). However, this conclusion is confounded by the observation that *Tnfrsf13b*$^{-/-}$ mice have elevated levels of BAFF in the serum (Bossen et al., 2008; Grasset et al., 2020; Sintes et al., 2017). Since the overexpression of BAFF leads to increased B cells (Mackay et al., 1999), the higher B cell numbers in TACI-deficient mice could be caused by elevated BAFF in the serum.

To extend these studies, we analyzed TACI-deficient mice and confirmed that they have a threefold increase in circulating levels of BAFF and increased numbers of both FO and MZ B cells in the spleen, although the increase is larger for FO B cells resulting in a decrease in the fraction of mature B cells that are MZ B cells (Fig. 1 A; and Fig. S1, C and D). In agreement with increased BAFF-induced signaling through BAFFR, TACI-deficient FO B cells had elevated levels of ICOSL, a known target of BAFFR signaling (Fig. S1 E) (Ou et al., 2012).

In view of the increased levels of BAFF, BAFFR signaling, and mature B cell numbers in TACI-deficient mice, it is not possible to analyze the cell-intrinsic role of TACI by comparing B cells from TACI-deficient and wild-type (WT) mice. To resolve this issue, we generated mixed bone marrow chimeras, reconstituting irradiated RAG1-deficient mice with bone marrow from either *Tnfrsf13b*$^{-/-}$ or *Tnfrsf13b*$^{+/+}$ mice expressing CD45.2 (CD45.2^{+}), mixed 50:50 with WT bone marrow from CD45.1^{+} mice, to generate KO:WT and WT:WT chimeras, respectively (Fig. 1 B). Both sets of chimeras had similar levels of serum BAFF, confirming that this approach eliminates the confounding factor of elevated BAFF (Fig. 1 C). In line with this, KO:WT chimeras did not display splenic B cell hyperplasia and TACI-deficient FO B cells from KO:WT chimeras had no change in ICOSL surface expression, consistent with unaltered BAFFR signaling (Fig. S2, A–C). These observations indicate that the B cell hyperplasia and increased ICOSL expression seen in *Tnfrsf13b*$^{-/-}$ mice are not cell-intrinsic effects of TACI loss, but more likely a consequence of increased levels of BAFF in the serum, and demonstrate that the mixed chimeras can be used to study the cell-intrinsic consequence of TACI deficiency.

Comparison of WT and TACI-deficient B cells taken from WT:WT and KO:WT chimeric mice showed that low levels of TACI expression can be detected on T1 and T2 B cells, with upregulation of TACI occurring as the cells mature into FO and MZ B cells (Fig. S2 D). MZ B cells express substantially more TACI compared with FO B cells, and even higher levels are seen on plasma cells.

Surprisingly, further analysis of the chimeras showed that the proportion of TACI-deficient CD45.2^{+} MZ B cells was reduced in KO:WT chimeras compared with WT CD45.2^{+} MZ B cells in WT:WT chimeras (Fig. 1 D and Fig. S2 A). In contrast, loss of TACI

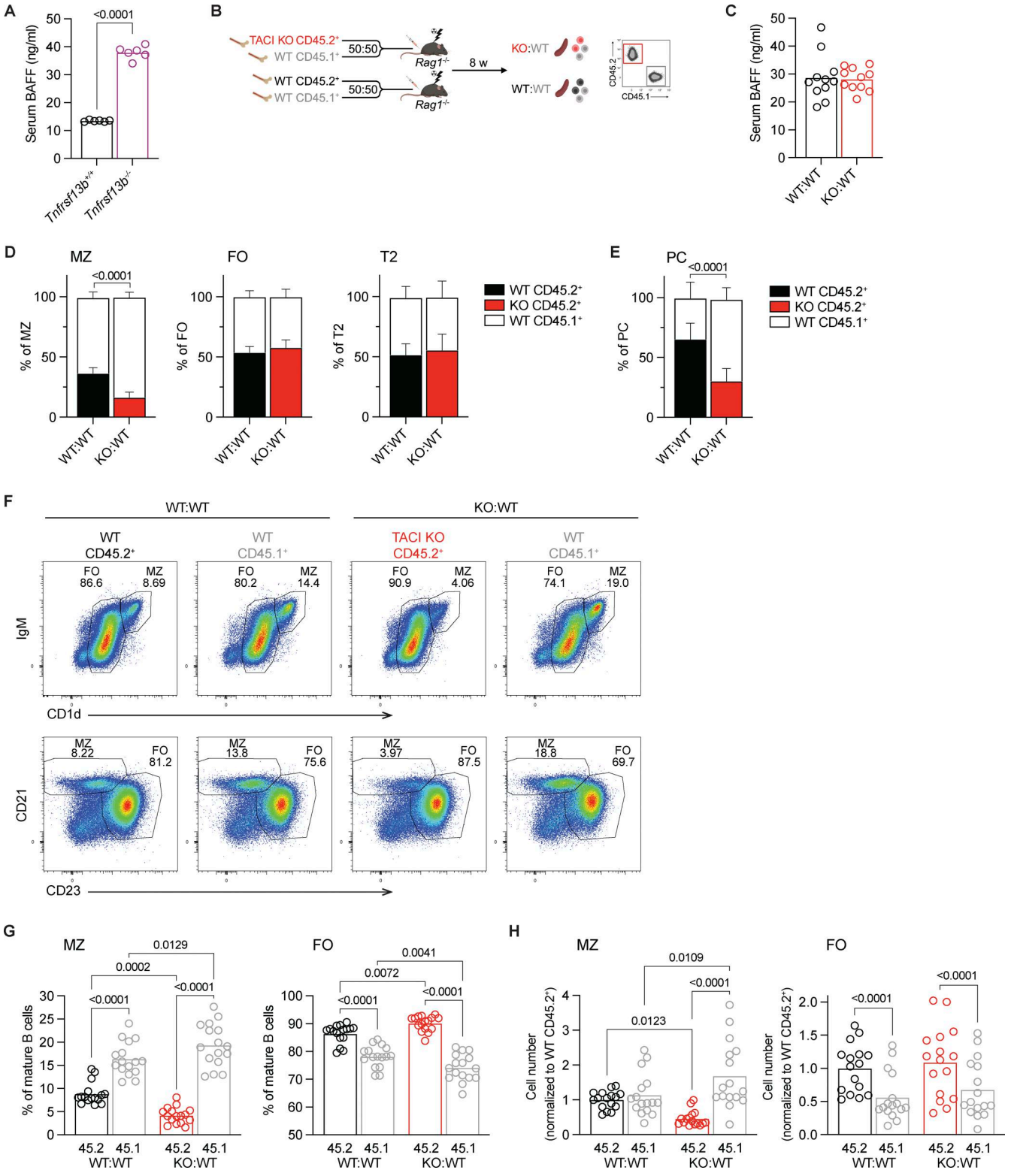

Figure 1. **TACI deficiency leads to reduced MZ B cells. (A)** Concentration of BAFF in the serum of *Tnfrsf13b*$^{+/+}$ and *Tnfrsf13b*$^{-/-}$ mice. Bars show the mean. Each point represents one mouse. **(B)** Mixed bone marrow chimera generation. Bone marrow from *Tnfrsf13b*$^{+/+}$ or *Tnfrsf13b*$^{-/-}$ littermates (expressing the CD45.2^{+} allele) was mixed 50:50 with bone marrow from WT CD45.1^{+} mice, then injected into sublethally irradiated *Rag1*$^{-/-}$ mice. B cells were analyzed at least 8 wk later. **(C)** Concentration of BAFF in the serum of WT:WT and KO:WT chimeras. Bars show the mean. Each point represents one mouse. **(D)** Stacked bar charts showing the percentages of CD45.2^{+} and CD45.1^{+} cells within the splenic MZ (CD93^{-}CD1d^{hi}IgM^{hi}), FO (CD93^{-}CD1d^{med}IgM^{+}), and T2 (CD93^{+}IgD^{+}IgM^{+}) B cell (B220^{+}CD19^{+}) populations in WT:WT and KO:WT chimeras. Cells were analyzed by flow cytometry using the gating strategy in Fig. S2 A. Bars show the mean ±95% CI. **(E)** Stacked bar chart showing the percentages of CD45.2^{+} and CD45.1^{+} cells within the splenic PC population (TCRβ^{-}CD138^{+}CD19^{lo}) in WT:WT and KO:WT chimeras. Bars show the mean ±95% CI. **(F)** Representative flow cytometry plots showing the proportions of MZ and FO B cells within the CD45.2^{+}

and CD45.1$^+$ mature splenic B cell populations (CD93$^-$B220$^+$CD19$^+$CD138$^-$) in WT:WT and KO:WT chimeras. MZ and FO cells are gated via two different approaches. Numbers indicate the percentage of cells in that gate. **(G and H)** Proportions (G) and numbers (H) of MZ (CD1d^{hi}IgM^{hi}) and FO (CD1d^{med}IgM$^+$) cells within the CD45.2$^+$ and CD45.1$^+$ mature splenic B cell populations (CD93$^-$B220$^+$CD19$^+$CD138$^-$) in WT:WT and KO:WT chimeras. Bars show the mean. Each point represents one mouse. Black: WT CD45.2$^+$; red: TACI KO CD45.2$^+$; gray: WT CD45.1$^+$. Statistical tests: Welch's *t* test (A and C), two-way ANOVA with Fisher's LSD test (D and E), repeated-measures two-way ANOVA with Fisher's LSD test (G and H). Numbers above graphs indicate P values where P ≤ 0.05, otherwise no value is shown. Sample numbers: 6 (A and D), 11 (C), 5 (E), 16 (G and H). Data are pooled from two experiments representative of four experiments (D), one out of two experiments (E), and pooled from six (A), five (C) and four (G and H) independent experiments. PC, plasma cell.

had no effect on the proportions of FO B cells or T2 B cells, the direct precursors of MZ and FO B cells. Analysis of splenic plasma cells showed that the proportion and number of TACI-deficient plasma cells were reduced (Fig. 1 E; and Fig. S2, A and E), in line with previous studies reporting the importance of TACI in plasma cell survival and differentiation (Eslami et al., 2024; Ou et al., 2012; Tsuji et al., 2011). Furthermore, within the TACI-deficient mature B cells, the proportion and absolute number of MZ B cells were reduced, while the proportion of FO B cells was increased, but the absolute number of FO B cells was not significantly changed (Fig. 1, F–H). Finally, loss of TACI had no effect on the numbers of T2 B cells (Fig. S2 F). These observations demonstrate that loss of TACI results in a cell-intrinsic reduction in the number of MZ B cells, with no effect on the numbers of FO or T2 B cells.

TACI is required for a T-independent antibody response

Given that MZ B cells are a major contributor to T-independent antibody responses (Li et al., 2022; Martin et al., 2001), we examined whether the reduction in TACI-deficient MZ B cells in KO:WT chimeras would impair this immune response. To do this, we reconstituted RAG1-deficient mice with bone marrow from either *Tnfrsf13b*$^{-/-}$ or *Tnfrsf13b*$^{+/+}$ C57BL/6 (B6) mice, this time mixed 50:50 with WT bone marrow from 129S7 (129) mice, generating KO:wt and WT:wt chimeras, respectively (Fig. 2 A). In these mixed chimeras, antibodies and B cells of B6 and 129 origins can be distinguished by IgH^b and IgH^a allotypes and by expression of Ly9.2 and Ly9.1, respectively. Once again, we found that the proportion and number of TACI-deficient MZ B cells were reduced in KO:wt chimeras compared with WT MZ B cells in WT:wt chimeras, whereas FO B cells were not affected (Fig. 2, B–E; and Fig. S2 G). We immunized the chimeras with trinitrophenyl (TNP)-Ficoll, an antigen that stimulates a T-independent antibody response, and 7 days later measured serum levels of TNP-specific IgM of both a and b allotypes (Fig. 2 A). We found that KO:wt chimeras had a greatly impaired IgM^b response compared with WT:wt chimeras, whereas the IgM^a response in the same mice originating from the 129-derived WT B cells was unaffected (Fig. 2 F). In line with this, we observed a reduced expansion of TACI-deficient plasma cells compared with WT plasma cells in response to immunization with TNP-Ficoll, and no expansion of TACI-deficient plasmablasts (Fig. 2, G and H; and Fig. S2 G).

The impaired T-independent antibody response is consistent with the reduction in MZ B cells in the absence of TACI, but it could also result from a defect in the ability of TACI-deficient MZ B cells to differentiate into antibody-secreting cells. To test this possibility, we sorted MZ B cells from WT:WT and KO:WT chimeras and activated them in vitro with LPS for 3 days to induce plasmablast differentiation (Fig. 2 I and Fig. S3 A). We found that TACI-deficient MZ B cells can differentiate into plasmablasts, but this is impaired to a small extent compared with WT MZ B cells (Fig. 2 J and Fig. S3 B). Together, these results suggest that the impaired T-independent antibody response originating from TACI-deficient B cells may be due to a combination of lower numbers of MZ B cells and their reduced differentiation into plasmablasts.

Finally, we extended this analysis by examining whether loss of TACI affects a TD immune response by immunizing WT:WT and KO:WT chimeric mice with 4-hydroxy-3-nitrophenylacetyl-chicken gamma globulin (NP-CGG) in alum and examining the germinal center response 7 days later. As expected, immunization resulted in increased numbers of NP-specific germinal center B cells, but this was not affected by loss of TACI, consistent with the normal numbers of FO B cells, which are major contributors to TD germinal center responses (Fig. S3, C and D).

TACI-deficient MZ B cells do not have a survival, homing, or localization defect

The reduction in splenic MZ B cells in the absence of TACI could be due to impaired development, homing, or survival. In view of the association of TACI with BAFFR, we hypothesized that TACI may regulate MZ B cell survival. To address this, we measured the turnover of MZ B cells in the mixed chimeras by administering 5-ethynyl-2′-deoxyuridine (EdU) to the mice continuously for 6 wk (Fig. 3 A). In the steady state, only newly generated pro- and pre-B cells in the bone marrow proliferate and incorporate EdU into their DNA. In agreement with this, treatment of the mice with EdU for just 4 h showed no labeling of immature or mature splenic B cell populations of either genotype, confirming that they were not dividing (Fig. 3 B; and Fig. S3, E and F). Thus, the accumulation of EdU$^+$ immature and mature B cells measures influx of newly generated EdU$^+$ B cells into the peripheral B cell pools, and given that these pools are maintained at a constant size, the rate of EdU$^+$ cell entry is also a measure of the rate of efflux by death or differentiation. We found that the accumulation of EdU$^+$ B cells in the immature T1, T2, and T3 B cell pools and the mature MZ and FO B cell pools was not affected by loss of TACI, demonstrating that the efflux of TACI-deficient MZ B cells from the MZ pool was unaltered and implying that TACI-deficient MZ B cells do not have a survival defect (Fig. 3 B; and Fig. S3, E and F). To extend this, we transferred splenic B cells from mixed chimeras into CD45.1$^+$CD45.2$^+$ recipient mice and analyzed the mice 7 days later (Fig. 3 C and Fig. S3 G). We found no differences in the recovery of TACI-deficient MZ or FO B cells compared with WT cells, supporting our conclusion that loss of TACI does not affect MZ B cell survival in vivo (Fig. 3 D). Finally, we examined the survival of TACI-deficient MZ B cells

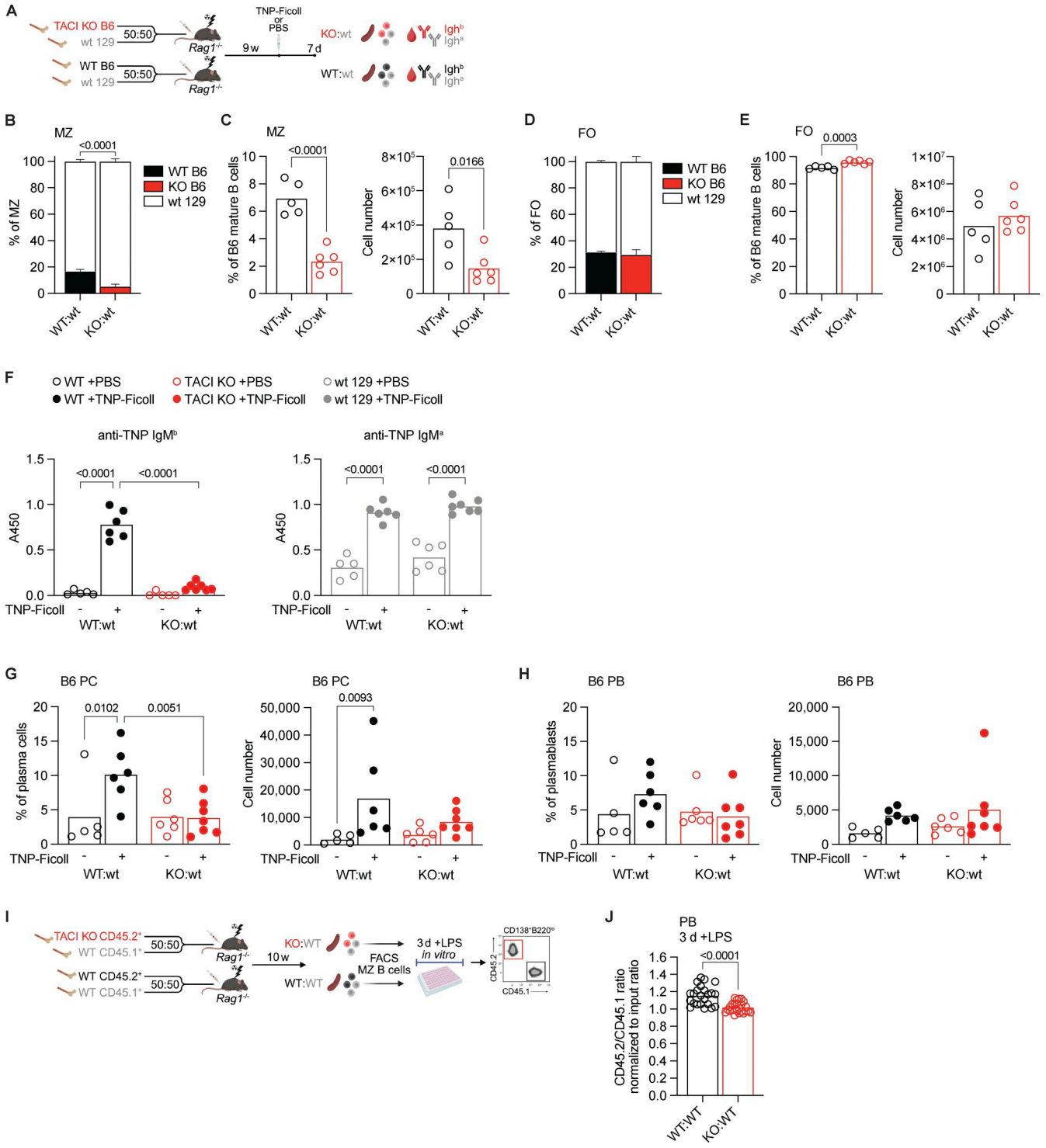

Figure 2. **TACI is required for T-independent antibody responses. (A)** Mixed bone marrow chimera generation for studies of T-independent antibody responses. Bone marrow from *Tnfrsf13b*$^{+/+}$ or *Tnfrsf13b*$^{-/-}$ littermates on the C57BL/6 (B6) background (Ly9.1^{-}) was mixed 50:50 with bone marrow from WT 129S7 (129) mice (Ly9.1^{+}), then injected into sublethally irradiated *Rag1*$^{-/-}$ mice, to generate WT:wt and KO:wt chimeras, respectively. 9 wk later, mice were injected i.p. with TNP-Ficoll or PBS as a control. 7 days after immunization, spleens and blood were harvested for analysis. Antibodies produced by C57BL/6 or 129S7 cells are of the Igh^{b} or Igh^{a} allotype, respectively. **(B)** Stacked bar chart showing the percentages of B6 and 129 cells within the total splenic MZ B cell populations (B220^{+}CD19^{+}CD93^{-}CD1d^{hi}IgM^{hi}) in WT:wt and KO:wt chimeras. Cells were analyzed by flow cytometry using the gating strategy shown in Fig. S2 G. Bars show the mean ±95% CI. **(C)** Proportion of MZ B cells (CD1d^{hi}IgM$^{b\ hi}$) within the B6 mature splenic B cell populations (Ly9.1^{-}CD93^{-}B220^{+}CD19^{+}CD138^{-}) and cell numbers in WT:wt and KO:wt chimeras. Bars show the mean. Each point represents one mouse. Black: WT B6; red: TACI KO B6. **(D)** Stacked bar chart showing the percentages of B6 and 129 cells within the total splenic FO B cell populations (B220^{+}CD19^{+}CD93^{-}CD1d^{med}IgM^{+}) in WT:wt and KO:wt chimeras. Cells were analyzed by flow cytometry using the gating strategy shown in Fig. S2 G. Bars show the mean +95% CI. **(E)** Proportion of FO B cells (CD1d^{med}IgM^{b+}) within the B6 mature splenic B cell populations (Ly9.1^{-}CD93^{-}B220^{+}CD19^{+}CD138^{-}) and cell numbers in WT:wt and KO:wt chimeras. Bars show the mean. Each

point represents one mouse. Black: WT B6; red: TACI KO B6. **(F)** TNP-specific IgM^b and IgM^a antibody responses in WT:wt and KO:wt chimeras 7 days after immunization with TNP-Ficoll or PBS control. IgM^b originates from B6 B cells (black: WT; red: TACI KO), whereas IgM^a originates from WT 129 B cells (gray). Antibody levels in serum were determined by ELISA and measured as absorbance at 450 nm (A450). Bars show the mean. Each point represents one mouse. **(G and H)** Percentage and numbers of B6 cells (Ly9.1$^-$) within the splenic PCs (TCRβ$^-$CD138$^+$B220^{lo}CD19$^{int\text{-}lo}$) (G) or PBs (TCRβ$^-$CD138$^+$B220^{hi}CD19^{int}) (H) in WT:wt and KO:wt chimeras 7 days after immunization with TNP-Ficoll or PBS control. Bars show the mean. Each point represents one mouse. Black: WT B6; red: TACI KO B6. **(I)** In vitro plasmablast differentiation assay. WT:WT and KO:WT mixed bone marrow chimeras were generated as in Fig. 1 B. MZ B cells (CD21^{hi}CD23^{lo}CD93$^-$CD138$^-$CD19$^+$) were purified from spleens by FACS 10 wk later, using the gating strategy shown in Fig. S3 A, then cultured with LPS for 3 days in vitro before analysis of generated plasmablasts. **(J)** Ratio of CD45.2$^+$ to CD45.1$^+$ PBs (CD138$^+$B220^{lo}) generated after 3 days of LPS stimulation of FACS-purified MZ B cells from WT:WT or KO:WT chimeras, normalized to the ratio of CD45.2$^+$/CD45.1$^+$ MZ B cells at day 0 (input). Cells were analyzed by flow cytometry as shown in Fig. S3 B. Bars show the mean. Each point represents one biological replicate. Statistical tests: unpaired *t* test (C, E, and J), two-way ANOVA with Fisher's LSD test (B, D, and F–H). Numbers above graphs indicate P values where P ≤ 0.05, otherwise no value is shown. Sample numbers: 5 (B–E, WT:wt; F–H, WT:wt +PBS; F, KO:wt +PBS IgM^b only), 6 (B–E, KO:wt; F–H, WT:wt +TNP-Ficoll, KO:wt +PBS except for IgM^b in F), 7 (F–H, KO:wt +TNP-Ficoll), 23 (J, WT:WT), 24 (J, KO:KO). Data are representative of two (B–H) or pooled from three (J) independent experiments. PCs, plasma cells; PBs, plasmablasts.

in vitro by culturing them in the presence or absence of BAFF. We found that loss of TACI did not affect the viability of MZ B cells either with or without BAFF (Fig. 3 E).

We next considered whether loss of TACI affected homing of MZ B cells to the spleen. To examine this, we repeated the adoptive transfer experiment but analyzed the recipient mice 1 h after transfer. We found that TACI-deficient MZ and FO B cells homed more efficiently to the spleen compared with WT cells (Fig. 3 F and Fig. S3 H). We extended this by examining the localization of TACI-deficient MZ B cells to the MZ using an in vivo pulse labeling approach, for which we injected chimeric mice intravenously with a PE-conjugated anti-CD19 antibody and harvested the spleens for analysis 5 min later. The MZ has more direct access to the blood compared with the follicles; thus, B cells in the MZ are labeled more efficiently with the antibody compared with B cells in follicles during this time (Castrillon et al., 2023; Cinamon et al., 2008). As expected, a larger fraction of MZ B cells were labeled with the anti-CD19 antibody compared with FO B cells (Fig. 3, G and H). However, there was no difference in the labeling efficiency between TACI-deficient and WT MZ B cells. Thus, loss of TACI does not impair homing of MZ B cells to the spleen or their localization to the MZ. Taken together, these results demonstrate that loss of TACI does not reduce the survival or homing of MZ B cells and instead suggest that the lower numbers of MZ B cells are most likely due to impaired development of MZ B cells from their immature T2 B cell precursors.

TACI regulates the transcriptome of MZ B cells

MZ and FO B cells develop from transitional T2 B cells in the spleen. Maturation of MZ B cells involves upregulation of CD1d, IgM, and CD21 and downregulation of CD23 and IgD surface expression (Fig. S4 A). In contrast, FO B cells decrease CD1d, IgM, and CD21 expression, increase IgD, and maintain high CD23 levels. Analysis of the expression of these proteins on TACI-deficient MZ B cells from KO:WT chimeras showed that in comparison with WT MZ B cells, they express less CD1d, IgM, and CD21 and more CD23 and IgD (Fig. 4, A and B). Thus, TACI-deficient MZ B cells are more FO-like and less MZ-like, although still clearly distinct from WT FO cells, and appear to be less mature MZ B cells.

To extend this analysis, we used RNA sequencing (RNAseq) to analyze the transcriptomes of TACI-deficient and WT MZ and FO B cells in KO:WT and WT:WT chimeras, including both the CD45.2$^+$ and CD45.1$^+$ B cells in the analysis (Fig. S4 B). Comparison of the transcriptomes of TACI-deficient and WT MZ B cells (CD45.2$^+$) revealed 686 differentially expressed genes (fold change >1.2, adjusted P value [padj] <0.05) (Fig. S4 C and Table S2). In contrast, no genes were differentially expressed when we compared control WT CD45.1$^+$ MZ B cells from KO:WT and WT:WT chimeras, and only 34 genes were differentially expressed between TACI-deficient and WT CD45.2$^+$ FO B cells (Fig. S4, D and E; and Table S2). Thus, loss of TACI selectively affects the transcriptome of MZ B cells, and not FO B cells, and the effect is cell intrinsic.

To investigate whether TACI-deficient MZ B cells had a less MZ-like and more FO-like identity, we generated transcriptional signatures of MZ and FO B cells from a comparison of WT MZ and WT FO B cells (Table S2). Gene set enrichment analysis (GSEA) showed that TACI-deficient MZ B cells had decreased expression of the MZ signature and increased expression of the FO signature (Fig. 4, C and D). Furthermore, in agreement with the changes in protein expression at the surface, transcripts encoding CD1d (*Cd1d1*) and CD21 (*Cr2*) were reduced and those encoding CD23 (*Fcer2a*) and IgD (*Ighd*) were increased in TACI-deficient MZ B cells (Fig. 4 E). Levels of transcripts encoding IgM (*Ighm*) were unchanged, implying that posttranscriptional mechanisms are likely to be responsible for the altered surface levels of IgM. Taken together, these data show that TACI-deficient MZ B cells are less MZ-like than WT MZ B cells and suggest that TACI regulates the development and maturation of MZ B cells from their T2 B cell precursors and the MZ versus FO B cell fate.

TACI-deficient MZ B cells have increased FOXO1 activity

To gain insights into how TACI may regulate the differentiation of MZ B cells, we investigated the effect of TACI deficiency on TF activity. Using GSEA to evaluate the expression of 475 TF target gene sets, we found that FOXO1 and FOXO3 target genes were among the most upregulated in TACI-deficient MZ B cells (Fig. 5 A and Table S2). In contrast, the expression of the target gene set of the NOTCH receptor, a key pathway and TF that promotes MZ B cell development (Pillai and Cariappa, 2009), was not significantly altered (Fig. 5 A). Additional GSEA using genes that are both bound and activated by FOXO1 in mouse lymphocytes (Table S2) showed increased expression of FOXO1-activated target genes in TACI-deficient MZ B cells (Fig. 5 B and Table S2). Furthermore, loss of TACI resulted in increased expression of *Cxcr4*, *Bach2*, *Klf2*, *Ccr7*, and *Cd55*, known FOXO1 targets in B and

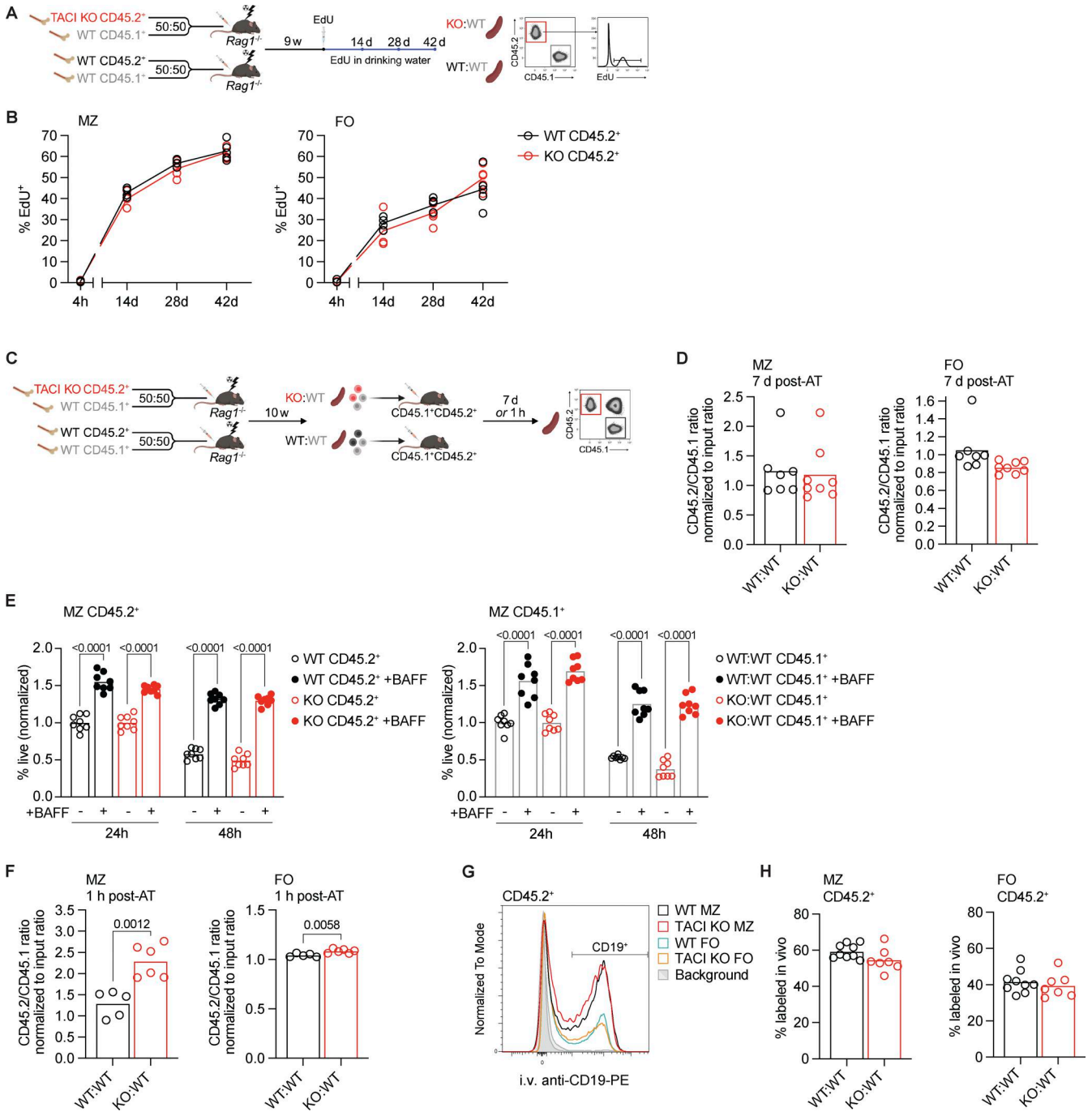

Figure 3. **TACI-deficient MZ B cells do not have a survival, homing, or localization defect. (A)** Schematic of in vivo continuous EdU labeling. WT:WT and KO:WT mixed bone marrow chimeras were generated as in Fig. 1 B. 9 wk later, mice were injected i.p. once with EdU, and then, EdU was maintained in drinking water for 42 days. Spleens were harvested at 4 h, and 14, 28, and 42 days following EdU injection. **(B)** Proportion of EdU$^+$ cells within MZ (CD1d^{hi}IgM^{hi}) and FO (CD1d^{med}IgM$^+$) CD45.2$^+$ mature splenic B cell populations (CD93$^-$B220$^+$CD19$^+$) from WT:WT and KO:WT chimeras at 4 h, 14, 28, and 42 days after start of EdU treatment. Cells were analyzed by flow cytometry using the gating strategy shown in Fig. S3 E. Each point represents one mouse (4 h WT, n = 4; KO, n = 5; 14 days, n = 4; 28 and 42 days, n = 5). Lines connect the mean at each time point. Black: WT CD45.2$^+$; red: TACI KO CD45.2$^+$. **(C)** Schematic of adoptive transfer. WT:WT and KO:WT mixed bone marrow chimeras were generated as in Fig. 1 B. At least 10 wk after reconstitution, splenic B2 cells were harvested from chimeras and transferred by i.p. injection into CD45.1$^+$CD45.2$^+$ recipients. Spleens of recipient mice were harvested either 7 days or 1 h later. The ratio of CD45.2$^+$/CD45.1$^+$ cells recovered was normalized to the ratio of CD45.2$^+$/CD45.1$^+$ cells in the injected mix (input). **(D)** Ratio of CD45.2$^+$ to CD45.1$^+$ MZ B cells (CD1d^{hi}IgM^{hi}CD93$^-$B220$^+$CD19$^+$) and FO B cells (CD1d^{med}IgM$^+$CD93$^-$B220$^+$CD19$^+$) recovered from the spleens of recipient mice 7 days after AT of B cells from WT:WT or KO:WT chimeras, normalized to the ratio of CD45.2$^+$ to CD45.1$^+$ MZ or FO B cells in the B cells that were transferred (input). Cells were analyzed by flow cytometry using the gating strategy shown in Fig. S3 G. Bars show the mean of n = 7 (WT:WT) and n = 8 (KO:WT) recipient mice. Each point represents one recipient mouse. **(E)** Viability of CD45.2$^+$ and CD45.1$^+$ MZ B cells (CD1d^{hi}IgM^{hi}CD93$^-$CD138$^-$B220$^+$CD19$^+$) from WT:WT or KO:WT chimeras after 24 or 48 h in vitro culture with or without 200 ng/ml BAFF, normalized to the mean viability in the absence of BAFF at 24 h within the same genotype and experiment. Bars show the mean of n = 8; each point represents a biological replicate. **(F)** Ratio of CD45.2$^+$ to CD45.1$^+$ MZ B cells (CD1d^{hi}IgM^{hi}CD93$^-$B220$^+$CD19$^+$) and FO B cells

(CD1d^{med}IgM$^+$CD93$^-$B220$^+$CD19$^+$) recovered from the spleens of recipient mice 1 h after adoptive transfer of B cells from WT:WT or KO:WT chimeras, normalized to the ratio of CD45.2$^+$ to CD45.1$^+$ MZ or FO B cells in the B cells that were transferred (input). Cells were analyzed by flow cytometry using the gating strategy shown in Fig. S3 H. Bars show the mean of n = 5 (WT:WT) and n = 6 (KO:WT) recipient mice. Each point represents one recipient mouse. **(G)** Flow cytometry histograms comparing in vivo labeling of splenic TACI KO and WT MZ and FO CD45.2$^+$ B cells from WT:WT and KO:WT chimeras 5 min after i.v. injection of anti-CD19-PE antibody. Red: TACI KO CD45.2$^+$ MZ; black: WT CD45.2$^+$ MZ; blue: WT CD45.2$^+$ FO; orange: KO CD45.2$^+$ FO; filled light and dark gray: background staining of MZ and FO CD45.2$^+$CD45.1$^+$ B cells, respectively, spiked in during *ex vivo* homogenization of spleens. **(H)** Percentage of splenic TACI KO and WT MZ and FO CD45.2$^+$ B cells labeled in vivo with anti-CD19-PE 5 min after i.v. injection of the antibody into WT:WT and KO:WT chimeras. Bars show the mean of n = 9 (WT:WT) and n = 7 (KO:WT) mice. Each point represents one mouse. Statistical tests: two-way ANOVA with Šídák's multiple comparisons test (B and E), unpaired t test (D, F, and H). Numbers above graphs indicate P values where P ≤ 0.05, otherwise no value is shown. Data are pooled from four (B) or two independent experiments (D–F and H). AT, adoptive transfer.

T lymphocytes (Fig. 5, C and D) (Chen et al., 2010; Dominguez-Sola et al., 2015; Kim et al., 2013; Ochiai et al., 2012; Ouyang et al., 2012; Spinelli et al., 2021; Tamahara et al., 2017; Webb et al., 2016). Flow cytometric analysis confirmed increased expression of CD55 on the surface of MZ B cells; however, levels of CXCR4 were unaltered suggesting that there is posttranscriptional regulation of this receptor (Fig. 5 E). In contrast, *Prdm1*, which is repressed by FOXO1 in B cells (Dominguez-Sola et al., 2015), was downregulated in TACI-deficient MZ B cells compared with WT MZ B cells (Fig. 5, C and D). Together, these results indicate that loss of TACI in MZ B cells results in elevated FOXO1 activity.

FOXO1 is inactivated by the serine/threonine kinases AKT1 and AKT2 (AKT). Active AKT translocates to the nucleus and phosphorylates FOXO1, leading to FOXO1 nuclear exclusion and cytosolic sequestration, thereby reducing the expression of FOXO1 target genes. Conversely, loss of AKT activity causes nuclear localization of FOXO1. Furthermore, it has been shown that AKT-mediated inactivation of FOXO1 is critical for MZ B cell development (Cox et al., 2023). Given the increased FOXO1 activity in TACI-deficient MZ B cells, we considered whether this may be caused by reduced AKT activation. We performed GSEA using sets of genes that are up- or downregulated in B cells following the expression of constitutively active AKT1 (Table S2) (Cox et al., 2023). This showed that most of the genes upregulated by AKT1 overactivation were downregulated in TACI-deficient MZ B cells, whereas genes downregulated by AKT1 overactivation were increased in expression (Fig. 5, F and G). These analyses indicate that loss of TACI results in decreased AKT activity and increased FOXO1 activity in MZ B cells, suggesting that TACI regulates the AKT-FOXO1 pathway required for MZ B cell development.

AKT-mTOR complex 1 signaling is impaired in TACI KO MZ B cells

Given the indication of reduced AKT1 activity in the absence of TACI, we examined phosphorylation of AKT (pAKT) at two sites required for its full activation, T308 and S473, in MZ B cells from KO:WT and WT:WT chimeras. We found that TACI-deficient MZ B cells had reduced resting levels of pAKT at both T308 and S473, compared with WT CD45.2$^+$ MZ B cells and with internal control WT CD45.1$^+$ MZ B cells, in line with reduced AKT activation (Fig. 6, A–D).

Besides FOXO1, a key effector of AKT is the mTOR complex 1 (mTORC1). AKT phosphorylates and inhibits TSC1 and TSC2, negative regulators of mTORC1, thereby promoting mTORC1 activity. Activated mTORC1 phosphorylates and activates S6K1, which in turn phosphorylates S6 ribosomal protein at S235 and S236 (pS6). Notably, a previous study showed that APRIL induces mTORC1 activation in human MZ B cells, most likely through TACI since the cells do not express BCMA (Sintes et al., 2017). Therefore, we examined whether mTORC1 signaling was impaired in TACI-deficient MZ B cells by measuring pS6, which is mTORC1-dependent in MZ B cells (Fig. S4 F). We found that TACI-deficient MZ B cells had reduced levels of pS6 compared with WT MZ B cells (Fig. 6, E and F). Thus, loss of TACI in MZ B cells results in reduced AKT and mTORC1 activity, suggesting that TACI regulates both kinases.

TACI associates with PI3K and mTOR

AKT activation is regulated by PI3K activity, and mice expressing kinase-inactive PI3Kδ, the dominant Class IA PI3K isoform in lymphocytes, lack MZ B cells (Okkenhaug et al., 2002). PI3Kδ activation by cell-surface receptors necessitates its recruitment to the plasma membrane where it generates phosphatidylinositol (3,4,5)-trisphosphate (PIP_3), which in turn recruits AKT to enable its phosphorylation and activation by PDK1. Thus, we hypothesized that TACI may regulate membrane localization of PI3Kδ. In agreement with this, we found that TACI was associated with both the p85α regulatory subunit and the p110δ catalytic subunit of PI3Kδ (Fig. 6 G). Given that loss of TACI results in impaired mTORC1 activation and that TACI was shown to interact with mTOR in human MZ B cells (Sintes et al., 2017), we examined whether TACI associates with mTOR in mouse MZ B cells, finding that it does (Fig. 6 G). Furthermore, since the adaptor MyD88 has been shown to bind to TACI and proposed to mediate the TACI-mTOR interaction (He et al., 2010; Sintes et al., 2017), we also probed for MyD88 in TACI immunoprecipitates, but were unable to detect this protein (Fig. 6 G). The association of TACI with p85α, p110δ, and mTOR was seen both in the absence and in the presence of exogenously added BAFF or APRIL and thus may be independent of ligand engagement by TACI. We cannot rule out that MZ B cells make autocrine BAFF or APRIL, although this is unlikely since the mRNA transcripts encoding these proteins are very low (<0.5 tpm) in MZ B cells (Table S2). Overall, these results suggest that TACI associates with PI3K and mTOR to regulate AKT and mTORC1 signaling.

Discussion

Our study of the BAFFR interactome revealed that TACI associates with BAFFR. Since the BAFFR-TACI interaction was

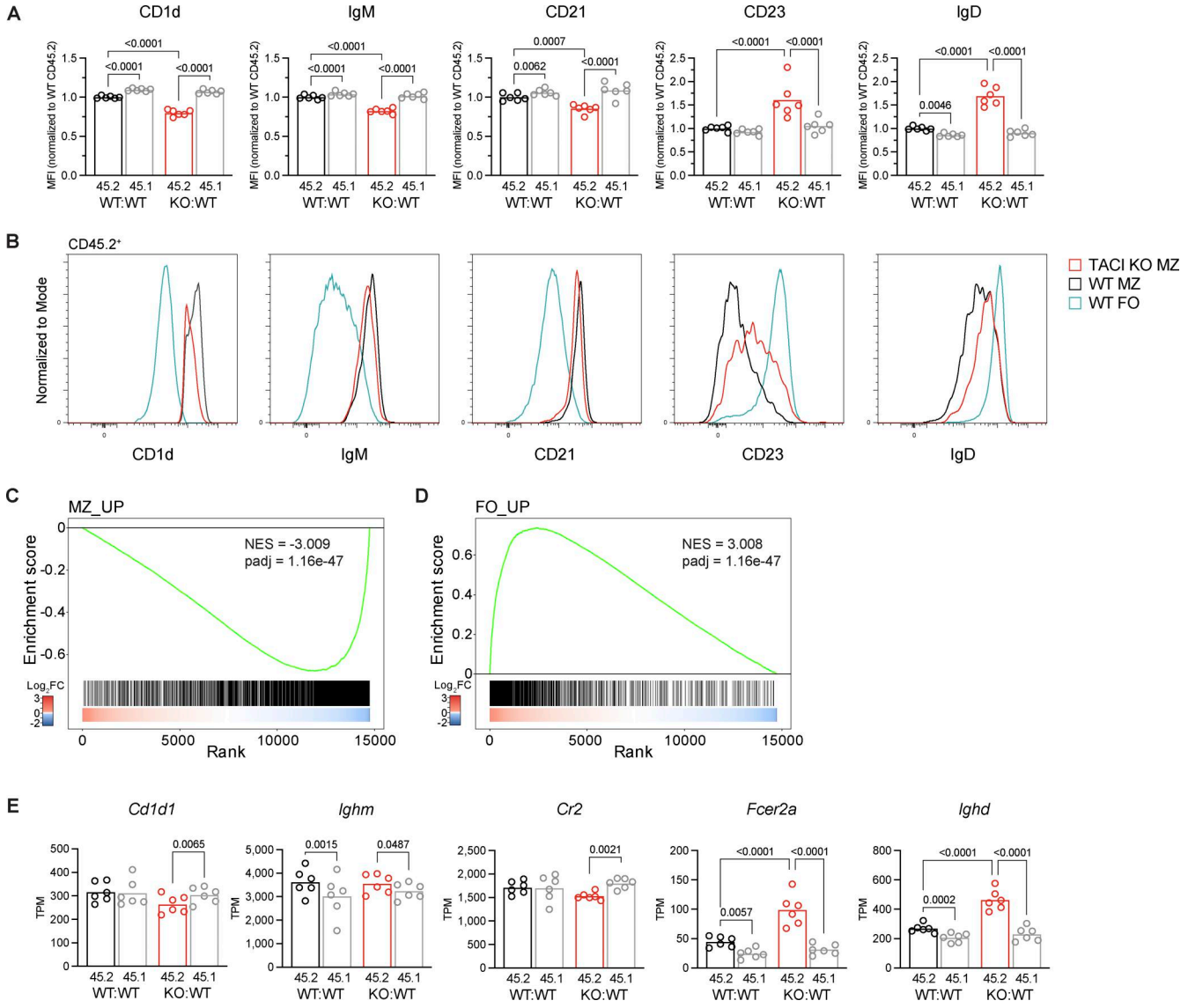

Figure 4. **TACI regulates the MZ B cell transcriptome. (A)** CD1d, IgM, CD21, CD23, and IgD surface expression, measured by flow cytometry, on CD45.2$^+$ and CD45.1$^+$ splenic MZ B cells (CD1d^{hi}IgM^{hi}CD93$^-$B220$^+$CD19$^+$) from WT:WT and KO:WT chimeras, quantified as the geometric MFI and normalized to the mean MFI of WT CD45.2$^+$ cells within the same experiment. Bars show the mean of data pooled from two independent analyses. Each point represents one mouse. Black: WT CD45.2$^+$; red: TACI KO CD45.2$^+$; gray: WT CD45.1$^+$. **(B)** Flow cytometry histograms comparing CD1d, IgM, CD21, CD23, and IgD surface expression on TACI KO and WT CD45.2$^+$ MZ B cells (CD1d^{hi}IgM^{hi}CD93$^-$B220$^+$CD19$^+$) and WT CD45.2$^+$ FO B cells (CD1d^{med}IgM$^+$CD93$^-$B220$^+$CD19$^+$) from WT:WT and KO:WT chimeras. Histograms are representative of the experiments quantified in A. Red: TACI KO CD45.2$^+$ MZ; black: WT CD45.2$^+$ MZ; blue: WT CD45.2$^+$ FO. **(C and D)** GSEA of the MZ signature (MZ_UP gene set) (C) and the FO signature (FO_UP gene set) (D) in TACI KO versus WT CD45.2$^+$ splenic MZ B cells. The plot shows the running enrichment score (green line) above the ranked list of genes, ordered from highest to lowest $\log_2$ fold change in TACI KO versus WT CD45.2$^+$ MZ B cells (red: upregulated; blue: downregulated; white: no change). The MZ_UP gene set comprises 2,339 genes significantly upregulated ≥1.5-fold in MZ B cells compared with FO B cells, and the FO_UP gene set comprises 1,321 genes significantly upregulated ≥1.5-fold in FO B cells compared with MZ B cells (WT CD45.2$^+$, from this study, Table S2). **(E)** *Cd1d*, *Ighm*, *Cr2*, *Fcer2a*, and *Ighd* mRNA expression in CD45.2$^+$ and CD45.1$^+$ splenic MZ B cells (CD1d^{hi}IgM^{hi}CD93$^-$B220$^+$CD19$^+$) from WT:WT and KO:WT chimeras, determined by RNAseq and quantified as TPM. Bars show the mean. Each point represents one mouse. Black: WT CD45.2$^+$; red: TACI KO CD45.2$^+$; gray: WT CD45.1$^+$. Statistical tests: repeated-measures two-way ANOVA with Fisher's LSD test. Numbers above graphs indicate P values where P ≤ 0.05, otherwise no value is shown. Sample numbers: 6 (A and E). MFI, mean fluorescence intensity; TPM, transcripts per million; NES, normalized enrichment score; padj, adjusted p-value.

dependent on the presence of BAFF, the interaction may be ligand-mediated. Both BAFFR and TACI form homotrimers that can bind trimeric BAFF. However, BAFF trimers can interact with each other to form higher order oligomers, a process that is essential for BAFF signaling through BAFFR (Vigolo et al., 2018). We speculate that such BAFF oligomers could simultaneously bind BAFFR and TACI trimers, thus bridging their interaction and promoting signaling through both receptors. Alternatively, BAFFR and TACI could interact directly. The functional consequence of the BAFFR-TACI interaction is unclear; it does not appear to be required for the survival of either FO or MZ B cells, as these are both unaffected by loss of TACI, but it may be

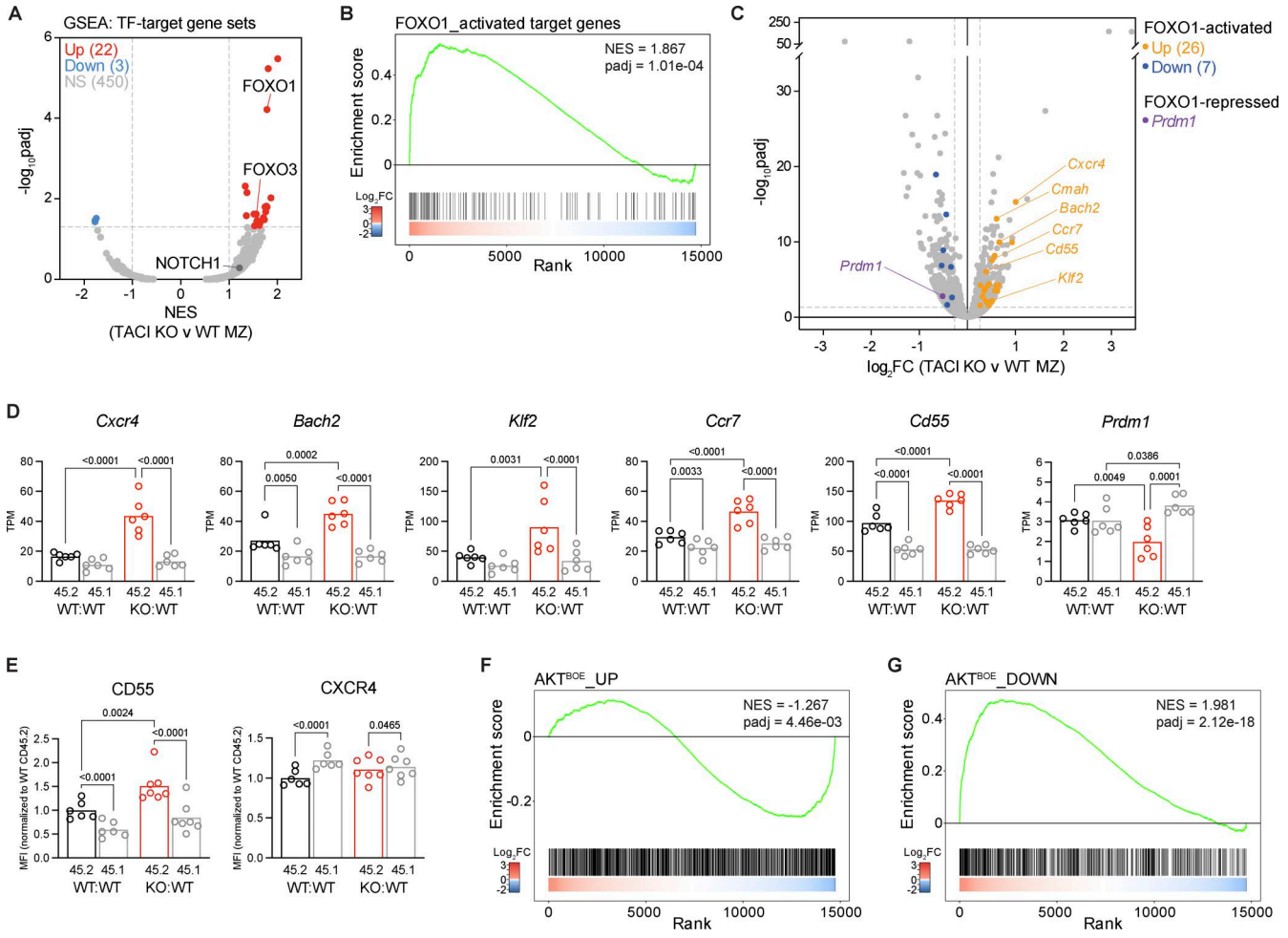

Figure 5. **Increased FOXO1 activity in TACI-deficient MZ B cells. (A)** Volcano plot of gene set enrichment in TACI KO versus WT CD45.2$^+$ MZ B cells for 475 TF target gene sets, showing the NES and $-\log_{10}$padj for each gene set determined by GSEA. Significantly differentially expressed TF target gene sets are in red (upregulated; NES ≥1, padj <0.05) and blue (downregulated; NES ≤−1, padj <0.05). Gray: not significantly differentially expressed (NS). Results for FOXO1, FOXO3, and NOTCH1 target gene sets are shown. **(B)** GSEA of FOXO1-activated target genes in TACI KO versus WT CD45.2$^+$ splenic MZ B cells. The plot shows the running enrichment score (green line) above the ranked list of genes, ordered from highest to lowest $\log_2$FC in TACI KO versus WT CD45.2$^+$ MZ B cells (red: upregulated; blue: downregulated; white: no change). The "FOXO1_activated target genes" gene set comprises 158 genes that are bound by FOXO1 in mouse lymphocytes and are downregulated following FOXO1 KO, curated as described in Materials and methods. **(C)** Volcano plot of differential gene expression between TACI KO and WT CD45.2$^+$ MZ B cells from KO:WT and WT:WT chimeras, respectively, with differentially expressed FOXO1-activated or FOXO1-repressed target genes highlighted (orange: FOXO1-activated and upregulated, $\log_2$FC ≥0.263, padj <0.05; blue: FOXO1-activated and downregulated, $\log_2$FC ≤ −0.263, padj <0.05; purple: FOXO1-repressed and downregulated). The mean $\log_2$FC in KO versus WT cells and $-\log_{10}$padj are shown for each gene from n = 6 mice. **(D)** *Cxcr4*, *Bach2*, *Klf2*, *Ccr7*, *Cd55*, and *Prdm1* mRNA expression in CD45.2$^+$ and CD45.1$^+$ splenic MZ B cells (CD1d^{hi}IgM^{hi}CD93$^-$B220$^+$CD19$^+$) from WT:WT and KO:WT chimeras, determined by RNAseq and quantified as TPM. Bars show the mean of n = 6 mice. Each point represents one mouse. Black: WT CD45.2$^+$; red: TACI KO CD45.2$^+$; gray: WT CD45.1$^+$. **(E)** CD55 and CXCR4 surface expression, measured by flow cytometry, on CD45.2$^+$ and CD45.1$^+$ splenic MZ B cells (CD1d^{hi}IgM^{hi}CD93$^-$B220$^+$CD19$^+$) from WT:WT and KO:WT chimeras, quantified as the geometric MFI and normalized to the mean MFI of WT CD45.2$^+$ cells within the same experiment. Bars show the mean of n = 6 (WT:WT) and n = 7 (KO:WT) mice, pooled from two independent analyses. Each point represents one mouse. Black: WT CD45.2$^+$; red: TACI KO CD45.2$^+$; gray: WT CD45.1$^+$. Statistical tests in D and E: repeated-measures two-way ANOVA with Fisher's LSD test. Numbers above graphs indicate P values where P ≤ 0.05, otherwise no value is shown. **(F and G)** GSEA of AKT-positively regulated genes (AKT^{BOE}_UP gene set) (F) and of AKT-negatively regulated genes (AKT^{BOE}_DOWN gene set) (G) in TACI KO versus WT CD45.2$^+$ splenic MZ B cells, displayed as in B. The AKT^{BOE}_UP gene set comprises 1,478 genes that are upregulated, and the AKT^{BOE}_DOWN gene set comprises 909 genes that are downregulated in B cells overexpressing constitutively activated AKT1 (AKT^{BOE}), compared with control B cells. MFI, mean fluorescence intensity; TPM, transcripts per million; $\log_2$FC, $\log_2$ fold change; NES, normalized enrichment score; padj, adjusted p-value.

required for effective signaling through TACI to regulate MZ B cell development.

Previous studies had shown that loss of TACI in mice leads to an increased number of both FO and MZ B cells, leading to the conclusion that TACI is a negative regulator of B cell survival (Shulga-Morskaya et al., 2004; von Bulow et al., 2001; Yan et al., 2001). However, since TACI-deficient mice have elevated levels of BAFF in the serum (Bossen et al., 2008; Grasset et al., 2020; Sintes et al., 2017), and overexpression of BAFF in mice leads to more B cells (Mackay et al., 1999), the increased number of B cells may be a direct consequence of higher serum BAFF. Our results with mixed chimeras support this conclusion: the KO:WT

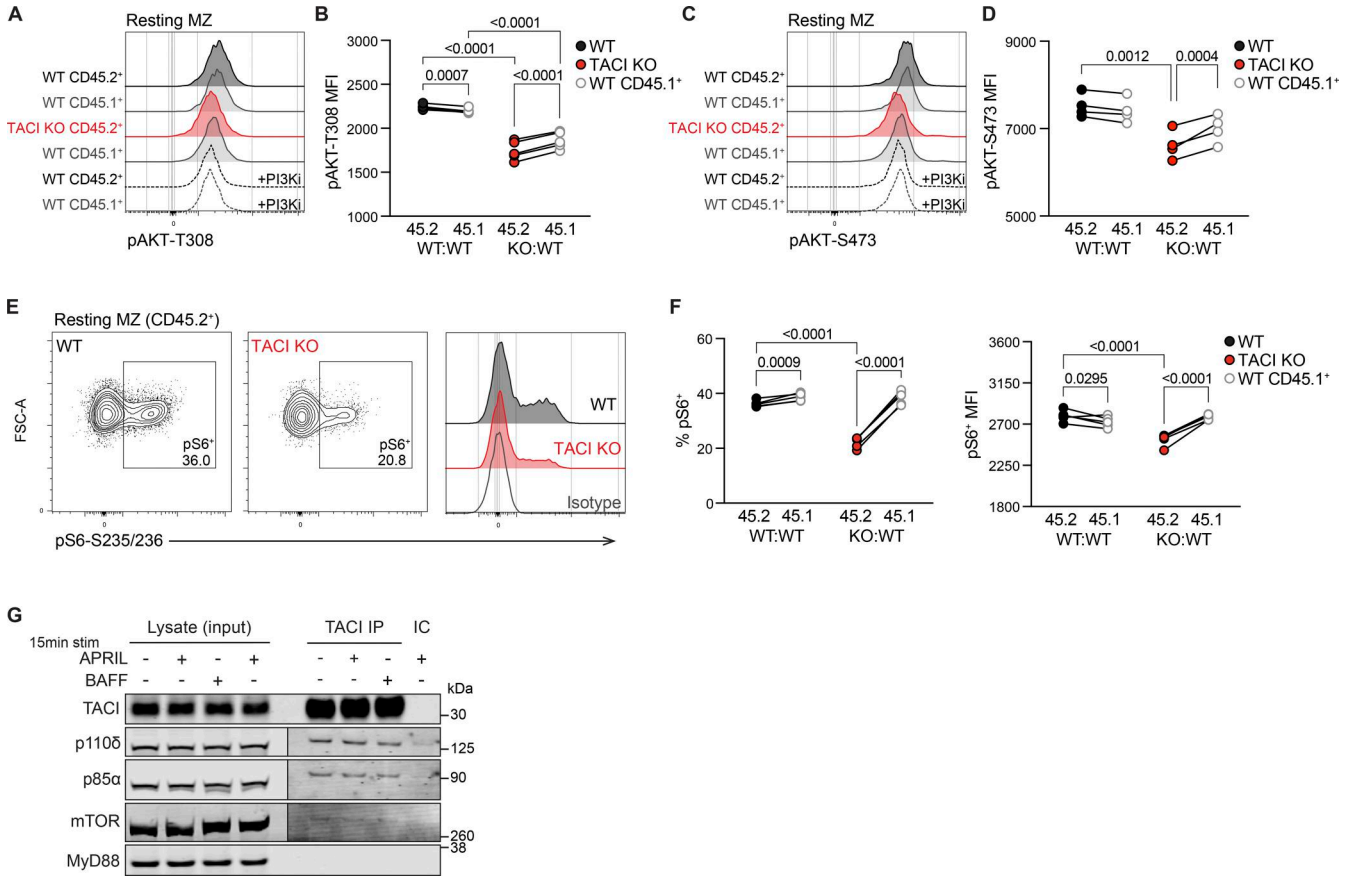

Figure 6. **AKT-mTORC1 signaling is impaired in TACI KO MZ B cells. (A)** Flow cytometry histograms comparing pAKT-T308 levels in TACI KO CD45.2⁺, WT CD45.2⁺, and WT CD45.1⁺ resting MZ B cells at 37°C from WT:WT and KO:WT chimeras. Red: TACI KO CD45.2⁺ MZ; black: WT CD45.2⁺ MZ; gray: WT CD45.1⁺; dashed lines: cells treated with the PI3Kδ inhibitor idelalisib (PI3Ki). **(B)** pAKT-T308 MFI, measured by flow cytometry, in CD45.2⁺ and CD45.1⁺ resting MZ B cells from WT:WT and KO:WT chimeras. WT:WT, *n* = 4; and KO:WT, *n* = 5. Lines connect cells from the same sample. Black: WT CD45.2⁺; red: TACI KO CD45.2⁺; gray: WT CD45.1⁺. **(C)** Flow cytometry histograms comparing pAKT-S473 levels in TACI KO CD45.2⁺, WT CD45.2⁺, and WT CD45.1⁺ resting MZ B cells at 37°C from WT:WT and KO:WT chimeras. Red: TACI KO CD45.2⁺ MZ; black: WT CD45.2⁺ MZ; gray: WT CD45.1⁺; dashed lines: cells treated with the PI3Kδ inhibitor idelalisib (PI3Ki). **(D)** pAKT-S473 MFI, measured by flow cytometry, in CD45.2⁺ and CD45.1⁺ resting MZ B cells from WT:WT and KO:WT chimeras; *n* = 4. Lines connect cells from the same sample. Black: WT CD45.2⁺; red: TACI KO CD45.2⁺; gray: WT CD45.1⁺. **(E)** Flow cytometry plots and histograms comparing pS6-S235/236 levels in WT and TACI KO CD45.2⁺ resting MZ B cells at 37°C from WT:WT and KO:WT chimeras. Black: WT CD45.2⁺; red: TACI KO CD45.2⁺; gray: WT cells stained with isotype control antibody (Isotype). **(F)** Percentage of pS6⁺ cells (left) and pS6 MFI within pS6⁺ cells (right), measured by flow cytometry, in CD45.2⁺ and CD45.1⁺ resting MZ B cells from WT:WT and KO:WT chimeras; *n* = 5. Lines connect cells from the same sample. Black: WT CD45.2⁺; red: TACI KO CD45.2⁺; gray: WT CD45.1⁺. **(G)** Immunoblot anti-TACI immunoprecipitation (IP) from LPS-activated B cells, alongside a control IP using isotype control antibody (IC) and the input cell lysates. Cells were stimulated with APRIL, BAFF, or media-only control for 15 min at 37°C. The immunoblot was probed with anti-TACI, anti-p110δ, anti-p85α, anti-mTOR, and anti-MyD88. The same membrane sections are displayed at two different image intensities for p110δ, p85α, and mTOR due to higher protein levels in the input lysates. Statistical test: repeated-measures two-way ANOVA with Fisher's LSD test (B, D, and F). Numbers above graphs indicate P values where P ≤ 0.05, otherwise no value is shown. Data are from one of four (B and F) or two (D and G) independent experiments. Source data are available for this figure: SourceData F6.

chimeras no longer had elevated levels of BAFF, B cell hyperplasia, or increased ICOSL expression, a hallmark of elevated BAFF-BAFFR signaling (Ou et al., 2012). The increase in serum BAFF in TACI-deficient mice may reflect a function of TACI as a decoy receptor for BAFF; ADAM10-mediated cleavage of TACI releases its extracellular domain, which can bind and sequester BAFF (Hoffmann et al., 2015; Smulski and Eibel, 2018). Alternatively, TACI may bind and internalize BAFF and target it for degradation, thereby contributing indirectly to B cell homoeostasis.

The analysis of mixed chimeras eliminated the elevated BAFF, B cell hyperplasia, and increased BAFFR signaling seen in TACI-deficient mice, allowing us to reveal a cell-intrinsic role of TACI. We show that loss of TACI leads to fewer MZ B cells because of impaired development of the cells from T2 B cell precursors. Surprisingly, TACI was not required for the survival of MZ or FO B cells. In line with this developmental role of TACI, the expression of the receptor is low on both T1 and T2 B cells and is upregulated strongly as they mature, especially in MZ B cells. Our results are supported by a previous study of mice expressing a TACI-Ig fusion protein, which binds and sequesters both BAFF and APRIL (Tardivel et al., 2004). These mice have very few FO or MZ B cells, as expected given the essential role of BAFF-BAFFR signaling in mature B cell survival. However, the ectopic expression of the anti-apoptotic protein BCL2 in these mice rescued FO B cell numbers, but not MZ numbers, indicating that BAFF and/or APRIL provide a survival-independent signal required

for the maturation of MZ B cells. We propose that this signal is mediated by TACI, though there may also be a contribution from BAFFR. In BAFFR-deficient and A/WySnJ (BAFFR-mutated) mice, which have very few mature B cells, the forced expression of BCL2 again restores numbers of FO but not MZ B cells, suggesting that BAFFR may also play a role in MZ development (Rahman and Manser, 2004; Sasaki et al., 2004). With respect to whether BAFF, APRIL, or both signal via TACI for MZ B cell development, we note that APRIL-deficient mice have normal numbers of MZ B cells (Varfolomeev et al., 2004). Similarly, mice expressing a BCMA-Ig fusion protein that binds and sequesters APRIL also have unaffected numbers of FO and MZ B cells (Schneider et al., 2001). BCMA is a third member of the TNF receptor subfamily that includes BAFFR and TACI, and binds APRIL but not BAFF. Taken together, these studies demonstrate that BAFF alone is sufficient to support TACI-dependent MZ B cell development. Further studies to support this conclusion would require the generation of mice with mutations that selectively affect BAFF binding to TACI without affecting the BAFF-BAFFR interaction critical for survival.

Our analysis of TACI-dependent signaling and gene expression in MZ B cells showed that loss of TACI results in reduced activation of AKT and increased FOXO1 activity. Given that AKT phosphorylates FOXO1 leading to its nuclear exclusion, the activation of FOXO1 in TACI-deficient MZ B cells is most likely due to reduced AKT activity, which will lead to increased active FOXO1 in the nucleus. The activation of AKT requires PI3K activity, and we show that TACI constitutively associates with the p85α regulatory subunit and p110δ catalytic subunit of PI3Kδ. It is unclear how this interaction is mediated, but it could involve the adaptor MyD88. MyD88 has been shown to interact with TACI and with BCAP, another adaptor protein that in turn binds p85 regulatory subunits of PI3K, so MyD88 could mediate this TACI-PI3Kδ interaction (He et al., 2010; Okada et al., 2000; Troutman et al., 2012). However, we could not detect an interaction between TACI and MyD88. Given that the BCAP-p85 interaction requires tyrosine phosphorylation of BCAP, the formation of a putative TACI-MyD88-BCAP-PI3K complex would require kinase activity. This could potentially be provided by BCR signaling leading to activation of the SYK kinase. Thus, we propose that TACI transduces signals via PI3K, localizing the enzyme at the plasma membrane where it can act on its substrate phosphatidylinositol (4,5)-bisphosphate to generate PIP_3, leading to AKT recruitment, activation, and subsequent FOXO1 inhibition.

Numerous previous studies support the importance of the PI3K-AKT-FOXO1 pathway in MZ B cell development. Mice expressing a kinase-inactive PI3Kδ lack MZ B cells (Okkenhaug et al., 2002), and deletion of both *Akt1* and *Akt2* in B cells results in a defect in MZ B cell development (Calamito et al., 2010). In contrast, mice expressing hyperactive PI3Kδ in B cells have increased MZ B cell numbers (Stark et al., 2018), while in those overexpressing constitutively membrane-localized and activated AKT1 in B cells, around 90% of splenic B cells are MZ B cells (Cox et al., 2023). The expression of a mutated FOXO1 that cannot be phosphorylated by AKT and hence is constitutively localized to the nucleus results in an almost complete lack of MZ B cells (Cox et al., 2023). Conversely, deletion of FOXO1 in B cells results in an increase in MZ B cells (Chen et al., 2010). One target gene through which FOXO1 may impact on MZ development is *Klf2*. FOXO1 directly binds to the *Klf2* gene, and FOXO1-deficient B cells have reduced *Klf2* expression (Chen et al., 2010; Webb et al., 2016). Importantly, mice with KLF2-deficient B cells have more MZ B cells and the remaining FO B cells are more MZ-like, implying that KLF2 may suppress MZ identity (Hart et al., 2011). In alignment with this, we showed that loss of TACI results in increased *Klf2* expression, which may in part account for the reduced numbers of MZ B cells, and for the remaining MZ B cells being less MZ-like. Taken together, these observations support our hypothesis that TACI-mediated activation of PI3K-AKT signaling and subsequent inhibition of FOXO1, resulting in reduced *Klf2* expression, are required for MZ B cell development from T2 B cells.

Several lines of evidence indicate that TACI signaling also activates mTORC1 in MZ B cells. Human and mouse MZ B cells exhibit higher TACI expression and mTORC1 signaling compared with FO B cells, and APRIL has been suggested to induce mTORC1 signaling in human B cells, most likely acting through TACI (Gaudette et al., 2020; Sintes et al., 2017). We now show that TACI-deficient mouse MZ B cells have lower basal mTORC1 signaling, in line with reduced AKT activity. Furthermore, we show that TACI associates with mTOR, an interaction that has been reported in human B cells (Sintes et al., 2017). Thus, TACI may promote mTORC1 activation in two ways: firstly, by bringing mTOR to the membrane; and secondly, by activating AKT, which subsequently phosphorylates and inhibits the negative regulators of mTORC1, TSC1, and TSC2. mTORC1 signaling may establish a poised state in MZ B cells that enables them to undergo rapid plasma cell differentiation (Gaudette et al., 2021; Sintes et al., 2017). mTORC1 regulates cell metabolism, including protein synthesis, as well as the expression of unfolded protein response genes, which are higher in MZ B cells in concordance with their plasma cell–primed state (Gaudette et al., 2020). Furthermore, mTOR-deficient mouse B cells show impaired class-switch recombination and plasmablast differentiation in vitro (Sintes et al., 2017). Our results support the notion that TACI contributes to the unique plasma cell–poised state of MZ B cells by promoting mTORC1 signaling. This may explain the reduced plasma cell differentiation of TACI-deficient MZ B cells, together with the reduced expression of *Prdm1* and the increased expression of *Bach2*, which promote and repress the generation of plasma cells, respectively (Kometani et al., 2013; Nutt et al., 2015).

The use of mixed chimeras demonstrated that loss of TACI results in reduced numbers of splenic plasma cells and an impaired T-independent antibody response. Interestingly, study of gut immune responses showed that TACI is also required for intestinal T-independent IgA responses and the generation of IgA^+ plasma cells (Grasset et al., 2020). Taken together, these defects in plasma cell numbers and T-independent antibody responses may be due to a combination of reduced MZ B cell numbers in the absence of TACI, as well as impaired plasma cell differentiation and plasma cell survival. The latter possibility is supported by previous studies showing that TACI contributes to plasma cell survival along with BCMA (Eslami et al., 2024; Ou et al., 2012).

Besides TACI, several other receptors also play important roles in MZ B cell development. BCR signaling is required for both FO and MZ B cell maturation, with MZ B cell development being dependent on BCRs with sufficient autoreactivity in order to meet the higher threshold of BCR signaling required to enter this compartment, compared with the FO compartment (Noviski et al., 2019; Wen et al., 2005). Deletion of the BCR coreceptor CD19, or mutation of its ICD to impair PI3K binding and activation, causes a near-complete loss of MZ B cells (Chen et al., 2010; Martin and Kearney, 2000; Wang et al., 2002). The NOTCH2 receptor also regulates the MZ fate, as loss of NOTCH2 in B cells results in a reduction of MZ B cells, whereas the ectopic expression of the NOTCH2 ICD causes a large expansion in MZ B cell numbers, in part because of transdifferentiation of FO B cells into MZ B cells (Hampel et al., 2011; Lechner et al., 2021; Saito et al., 2003). Notably, the expression of the NOTCH2 ICD results in reduced expression of *Foxo1* and *Klf2* (Lechner et al., 2021). Given that the BCR, CD19, and NOTCH2 activate PI3K and AKT (Aiba et al., 2008; Bailis and Pear, 2012; Castello et al., 2013; Gentle et al., 2012; Otero et al., 2001), these receptors may act in concert with TACI, converging on the same pathways that regulate MZ B cell development. Such a functional overlap may explain why some MZ B cells can still develop in the absence of TACI; however, BCR, CD19, and NOTCH2 are not sufficient for their full maturation since TACI-deficient MZ B cells are less MZ-like. Further work will be needed to understand how signals from these receptors intersect and their relative contributions to MZ B cell development.

Human MZ B cells have many similarities to mouse MZ B cells. They develop from bone marrow progenitors that emigrate and mature into MZ B cells under the influence of NOTCH2 and AKT signaling, localize to the splenic MZ, upregulate TACI as they mature, express higher levels of TACI compared with FO B cells, and are poised to differentiate into plasma cells, although unlike mouse cells, human MZ B cells circulate in the blood and may have higher levels of somatic hypermutation (Cox et al., 2023; Descatoire et al., 2014; Sintes et al., 2017; Siu et al., 2022; Tull et al., 2021). Thus, it seems likely that TACI signaling via AKT and FOXO1 also contributes to human MZ B cell development.

In summary, our results uncover a previously hidden role of TACI in MZ B cell development from T2 B cells. We show that loss of TACI reduces MZ B cell numbers, impairs the T-independent antibody response, and dysregulates the transcriptional programs distinguishing MZ and FO B cells. We propose that TACI regulates MZ development through promoting the PI3K-AKT pathway leading to inhibition of FOXO1 and reduced *Klf2* expression. Our work positions TACI among key receptors, alongside the BCR and NOTCH2, which govern the cell-fate decision between FO and MZ B cells, and broadens our view of the roles played by members of the TNF receptor superfamily in the establishment and maintenance of the mature B cell repertoire.

Materials and methods

Mice

Mice with the following alleles have been described previously: *Tnfrsf13b*^{tm1Vmd} (*Tnfrsf13b*$^{-}$, TACI KO), *Rag1*^{tm1Mom} (*Rag1*$^{-}$) (Mombaerts et al., 1992; Yan et al., 2001). Mice expressing a tagged BAFFR-Twin-Strep-tag (*Tnfrsf13c*^{em1Tyb}, *Tnfrsf13c*$^{Twin\text{-}Strep\text{-}tag}$) were generated using CRISPR/Cas9 gene editing to introduce a mutation that adds 32 amino acids to the C terminus of BAFFR, encoding a linker and two Strep-tag II sequences separated by another linker (amino acid sequence: 172-GPEQGGGSWSHPQFEKGGGSGGGSGGGSWSHPQFEK*-208; DNA sequence: 5′-GGCCCAGAGCAAGGTGGAGGATCTTGGAGCCACCCTCAATTCGAGAAGGGTGGAGGCAGTGGCGGGGGTTCTGGCGGCGGTTCATGGTCCCACCCCCAGTTTGAAAAATAGCCTTGCCGAGGCCATGGCAGCAGTGGA-3′; underlined is inserted, and nonunderlined is WT) (Fig. S1 A). TACI KO mice were on a C57BL/6NCrl background and maintained by intercrossing heterozygous mutants, taking homozygous mutant and WT littermate mice for experiments. RAG1 KO and BAFFR-Twin-Strep-tag mouse strains were backcrossed ≥10 generations onto the C57BL/6J (B6) background. B6 (CD45.2^{+}Ly9.1^{-}), B6.SJL-*Ptprc*^{a} *Pepc*^{b}/BoyJ (CD45.1^{+}), and 129S7 (129, CD45.2^{+}Ly9.1^{+}) strains were maintained as inbred strains by the Francis Crick Institute Biological Research Facility, who also generated (B6 × B6.SJL)F1 (CD45.1^{+}CD45.2^{+}) hybrid mice.

Mice were housed in specific pathogen-free conditions with up to 5 mice per individually ventilated cage (floor area 500 cm^{2}; Tecniplast) with bedding, nesting, and enrichment (Aspen 4HK, Bed-R'Nest; Datesand) at 21 ± 2°C and 55 ± 10% relative humidity in a 12/12-h light/dark cycle. Mice were fed 2018 Teklad Global Diet (Envigo; autoclaved) and supplied RO-filtered mains drinking water, ad libitum. Both female and male mice were used, with sexes balanced between different genotypes or conditions. All procedures were conducted in accordance with the United Kingdom Animals (Scientific Procedures) Act 1986, approved by the Francis Crick Institute Animal Welfare and Ethical Review Body and conducted under authority of a Project Licence issued by the UK Home Office.

Mixed bone marrow chimeras

Bone marrow was isolated from femurs and tibias in IMDM (in-house, with 0.06 mg/ml penicillin, 0.1 mg/ml streptomycin, pH 7.2) supplemented with 5% FCS, and then, red blood cells were lysed with ACK Lysing Buffer (Gibco) for 2 min at room temperature. T cells were depleted by incubation with biotinylated anti-CD3ε (100304; BioLegend; 2.5 µg/ml) for 20 min on ice and then with streptavidin-conjugated Dynabeads (M-280; Thermo Fisher Scientific; 1 × 10^{6} beads per 1 × 10^{6} cells) for 20 min at 4°C with rotation, followed by removal of the bead-bound cells with a magnet, washing, and resuspension in IMDM without FCS. T cell–depleted bone marrow from *Tnfrsf13b*$^{+/+}$ (WT) or *Tnfrsf13b*$^{-/-}$ (TACI KO) littermates was mixed 50:50 with bone marrow from either two to three B6.SJL (CD45.1^{+}) mice, for B6:B6.SJL (CD45.2^{+}:CD45.1^{+}) chimeras, or one 129S7 mouse, for B6:129 (Ly9.1^{-}:Ly9.1^{+}) chimeras. 100 µl of bone marrow mix at 2 × 10^{7} cells/ml was then injected into the tail vein of each *Rag1*$^{-/-}$ recipient, which had been irradiated with a sublethal dose of 5 Gy from a ^{137}Cs source at least 3 h earlier. Donor and recipient mice were sex-matched and aged 8–14 or 7–10 wk, respectively. Recipients received 0.02% enrofloxacin (Baytril, Bayer Healthcare) in their drinking water for 4 wk, and mixed chimeras were

analyzed at least 8 wk after bone marrow injection to allow the hematopoietic compartment to reconstitute.

Flow cytometry and cell sorting

Spleens were harvested and homogenized through 40-µm cell strainers with ice-cold fluorescence-activated cell sorting (FACS) buffer (PBS [Ca^{2+}/Mg^{2+}-free], 0.5% BSA [A2153, Sigma-Aldrich], 2 mM EDTA), and then, red blood cells were lysed with ACK Lysing Buffer for 2 min at room temperature. For flow cytometric analyses of splenocytes from chimeras, unless otherwise specified, cells were stained with viability dye diluted 1:500 in PBS at 2 × 10^7 cells/ml for 20 min at 4°C, then incubated with fluorophore-conjugated antibodies specific for surface markers diluted 1:200 in FACS buffer at 2 × 10^7 cells/ml for 30 min at 4°C, fixed in 100 µl Cytofix/Cytoperm (554722; BD Biosciences) for 15 min on ice, and analyzed in FACS buffer containing a set number of Calibrite beads (664912; BD Biosciences) on an Aurora spectral flow cytometer (Cytek). All antibody incubations included anti-CD16/32 (101302; BioLegend) to block Fc receptor binding. To detect surface CXCR4, splenocytes were rested for 2 h at 37°C in RPMI 1640 media supplemented with 0.5% heat-inactivated FCS before staining. Fluorophore-conjugated reagents used were as follows: B220-PerCP-Cy5.5 (RA3-6B2), B220-BV785 (RA3-6B2), B220-BV650 (RA3-6B2), CD138-BV785 (281-2), CD19-BV785 (6D5), CD19-APC (6D5), CD1d-APC (1B1), CD1d-PE (1B1), CD1d-BV421 (1B1), CD3ε-biotin (145-2C11), CD23-BV605 (B3B4), CD23-PE-Cy7 (B3B4), CD45.1-BV605 (A20), CD45.2-BV650 (104), CD45.2-BV785 (104), CD45.2-PerCP-Cy5.5 (104), CD93-PE-Cy7 (AA4.1), CXCR4-BV421 (L276F12), IgD-BV711 (11-26c.2a), IgD-AF647 (11-26c.2a), IgD-BV785 (11-26c.2a), IgM-BV510 (RMM-1), IgM[a]-PerCP-Cy5.5 (MA-69), IgM[b]-PE (AF6-78), streptavidin-BV570, streptavidin-PE-Cy7, TCRβ-AF700 (H57-597), and Zombie Aqua Fixable Viability Dye, all from BioLegend; B220-RB780 (RA3-6B2), CD19-BUV395 (1D3), CD19-APCeF780 (1D3), CD1d-BV605 (1B1), CD2-BV711 (RM2-5), CD95-PE-CF594 (Jo2), TACI-BV421 (8F10), CD3-BUV395 (2C11), CD93-BUV737 (AA4.1), CD138-BV711 (281-2), GL7-FITC, IgD-BV786 (11-26c.2a), IgD[a]-FITC (AMS9.1), IgM-BUV563 (II/41), IgM-BV605 (II/41), Ly9.1-BUV563 (30C7), and TCRβ-BUV395 (H57-597) all from BD Biosciences; B220-APC (RA3-6B2), BAFFR-FITC (eBio7H22-E16), CD21-APC-eF780 (8D9), CD38-PE-Cy5 (90), CD45.1-PerCP-Cy5.5 (A20), CD45.2-FITC (104), CD93-APC (AA4.1), F4/80-biotin (BM8), ICOSL-eF660 (B7-H2), TCRβ-APC-eF780 (H57-597), DAPI (used at 0.1 µg/ml with 10 min incubation), and Live/dead Fixable Near-IR Dead Cell Stain Kit (L10119) from Thermo Fisher Scientific; IgM-APC-ef780 (II/41) from eBioscience; NP-PE (N-5070) from LGC Biosearch Technologies; and CD55-APC (REA300) from Miltenyi Biotec.

For isolation of B cell populations by FACS for RNAseq and in vitro differentiation assays, B2 cells were first isolated from splenocyte single-cell suspensions by negative depletion using anti-CD43 MicroBeads (130-049-801; Miltenyi Biotec) and LS magnetic columns (Miltenyi Biotec), according to the manufacturer's protocol. B cells were stained with viability dye and fluorophore-conjugated antibodies, then sorted live using a FACSAria III or Fusion (BD Biosciences) into cold RPMI 1640 media (R8758; Sigma-Aldrich) supplemented with 10% heat-inactivated FCS, 100 U/ml penicillin, 100 µg/ml streptomycin, 2 mM L-glutamine (Sigma-Aldrich), and 50 µM β-mercaptoethanol (Thermo Fisher Scientific).

To label B cells in vivo, chimeras were injected into the tail vein with 200 µl PBS containing 1 µg anti-CD19-PE antibody (1D3, 152408; BioLegend) and culled 5 min later. Spleens were harvested and immediately homogenized on ice, with freshly harvested $CD45.1^+CD45.2^+$ splenocytes spiked into the single-cell suspension to serve as a background control accounting for antibody binding to cells *ex vivo*.

Immunizations

For TNP-Ficoll immunizations, at 9 wk after reconstitution, B6:129 (WT:wt and KO:wt) chimeras were injected intraperitoneally with 50 µg of TNP-Ficoll (F-1300, LGC Biosearch Technologies) in 200 µl PBS, or PBS only. For NP-CGG immunizations, at 10–12 wk after reconstitution, WT:WT and KO:WT chimeras were injected intraperitoneally with 50 µg of NP-CGG (N-5055C; LGC Biosearch Technologies) in 200 µl PBS containing 25% alum (77161; Thermo Fisher Scientific), or PBS with alum only. At day 7, spleens were harvested, and blood was collected by cardiac puncture into serum gel CAT tubes (41.1378.005; Sarstedt) and allowed to clot at room temperature for 1–2 h. Serum was isolated by centrifugation at 10,000 × *g* for 10 min at room temperature. Splenocytes were incubated with antibodies against cell-surface markers and viability dye for 30 min at 4°C, fixed with 250 µl Cytofix buffer (554655; BD Biosciences) for 20 min at 4°C, and analyzed in FACS buffer containing a set number of Calibrite beads on a Fortessa Symphony A5 (BD Biosciences).

ELISA

For the analysis of TNP-specific antibodies in serum by ELISA, 96-well MaxiSorp flat-bottom plates (439454; Thermo Fisher Scientific) were coated with 0.5 µg TNP-BSA (T-5050; LGC Biosearch Technologies) in 100 µl PBS overnight at 4°C followed by 1 h at room temperature and then washed five times with PBST (PBS, 0.01% Tween-20). Wells were blocked with 100 µl 3% BSA in PBS for 2 h at room temperature, then washed twice with PBST before the addition of serially diluted serum in 3% BSA in PBS and incubation for 2 h at room temperature. Wells were washed five times before the addition of 0.1 µg biotinylated anti-IgM[a] (553515; BD Biosciences) or anti-IgM[b] (406204; BioLegend) in 100 µl PBST and incubation for 2 h at room temperature. Wells were washed five times before the addition of 0.2 µg streptavidin-HRP (SA-5004-1; Vector Laboratories) in 100 µl PBST and incubation for 2 h at room temperature. Wells were washed five times, then incubated with 70 µl TMB substrate (00-4201; Thermo Fisher Scientific) until color developed, and the reaction was stopped with 70 µl 2N H_2SO_4. Absorbance at 450 nm was measured using a Spark microplate reader (Tecan). Antibody titer was recorded as the absorbance at a dilution in the linear section of the titration curve (1:1,600 for IgM^a and 1:200 for IgM^b).

The concentration of BAFF in serum was measured by ELISA using Mouse BAFF ELISA Kit (ab119580; Abcam) according to the manufacturer's instructions, with serially diluted serum incubated in anti-BAFF–coated plates overnight at 4°C and washes performed with PBST. Absorbance at 450 nm was

measured using a Spark microplate reader, and BAFF concentration was calculated using a standard curve generated with recombinant BAFF.

EdU labeling in vivo

At 9 or 12 wk after reconstitution, WT:WT and KO:WT chimeras were injected once intraperitoneally with 100 µl PBS containing 1 mg/ml EdU (F463473; Fluorochem), then received 0.3 mg/ml EdU in their drinking water for the duration of the time course, with EdU replenished every 3 days. Spleens were harvested at 4 h, 14, 28, and 48 days after injection, to analyze FO and MZ cells, or at 4 h, 2, 3, and 5 days after injection to analyze transitional B cells.

To analyze EdU$^+$ cells by flow cytometry, spleens were harvested, red blood cells were lysed, and splenocytes were incubated with antibodies against cell-surface markers and viability dye for 30 min at 4°C. Cells were washed, then fixed with 4% paraformaldehyde for 15 min at 4°C, and permeabilized in Perm/Wash Buffer (554723; BD Biosciences) supplemented with 1% BSA for 15 min at room temperature, before the addition of click reaction mix to a final concentration of 2 mM $CuSO_4$, 0.3125 µM AZDye 488 picolyl azide, and 10 mM sodium ascorbate (all from Jena Bioscience) in TBS (50 mM Tris, 150 mM NaCl, pH 7.5) and incubation for 30 min in the dark at room temperature. Cells were washed twice, then analyzed in Perm/Wash Buffer on a Fortessa Symphony A5.

Adoptive transfer of B cells

At 10–15 wk after reconstitution, spleens were harvested from two to three WT:WT and KO:WT chimeras, red blood cells were lysed, and B2 cells were isolated by negative depletion using anti-CD43 MicroBeads and LS magnetic columns, according to the manufacturer's protocol, and pooled by genotype. For 7-day adoptive transfer experiments, 1×10^7 purified B cells from WT:WT or KO:WT chimeras in 100 µl IMDM were injected intravenously into each sex-matched CD45.1$^+$CD45.2$^+$ recipient mouse. For 1-h adoptive transfer experiments, purified B cells were first incubated with 1 µM CMFDA (C7025; Thermo Fisher Scientific) in PBS for 10 min at 37°C, excess dye was quenched with IMDM containing 10% FCS for 7 min at 37°C, cells were washed, then 1×10^7 CMFDA-labeled B cells from WT:WT or KO:WT chimeras in IMDM were injected into each sex-matched CD45.1$^+$CD45.2$^+$ recipient. In each case, a proportion of the transferred cell suspension was analyzed by flow cytometry to determine the input ratio of CD45.2$^+$/CD45.1$^+$ cells among the FO and MZ B cells injected.

Recipient spleens were harvested 1 h or 7 days after adoptive transfer, red blood cells were lysed, and B2 cells were isolated by negative depletion using anti-CD43 MicroBeads and LS magnetic columns, as described before. Cells were incubated with antibodies against cell-surface markers and viability dye for 30 min at 4°C, fixed with 250 µl Cytofix buffer for 20 min at 4°C, and analyzed in FACS buffer containing a set number of Calibrite beads on a Fortessa Symphony A5. The ratio of CD45.2$^+$/CD45.1$^+$ cells among the FO and MZ B cells recovered was divided by the corresponding ratio of CD45.2$^+$/CD45.1$^+$ cells in the FO and MZ populations that were transferred.

RNAseq

Cell pellets were lysed after FACS in Buffer RLT (QIAGEN) with 500 µM β-mercaptoethanol, then frozen until processing. Lysates were homogenized using QIAshredder spin columns, and then, RNA was extracted using the RNeasy Mini or Micro kit (QIAGEN) with DNase digestion on a QIAcube Connect, all according to the manufacturer's instructions. cDNA libraries were generated using the Watchmaker RNA Library Prep Kit with Polaris Depletion of rRNA and globin transcripts according to the manufacturer's instructions. Libraries were sequenced on the Illumina NovaSeq X, acquiring 25 million 100-bp paired-end reads per sample.

Alignment of paired-end raw reads was performed with the nf-core rnaseq pipeline v3.6 using the star rsem aligner option and the ENSEMBL GRCm39 release 105 transcriptome (https://zenodo.org/records/15631172). Differential gene expression analysis was performed using the DESeq2 R package, where padj were calculated using the Benjamini–Hochberg method, with a significance threshold of padj <0.05 (Love et al., 2014). GSEA were performed using the FGSEA R package with genes preranked according to $\log_2$ fold change (Korotkevich et al., 2021, *Preprint*). GSEA normalized enrichment scores (NES) were computed by permutation testing (1,000 permutations), and padj were calculated using the Benjamini–Hochberg multiple testing correction, with a significance threshold of padj <0.05. Gene sets used for GSEA were curated as follows: TF target gene sets were curated using the OmniPath Python package (Turei et al., 2021). FOXO1-activated target genes were manually curated by cross-referencing FOXO1 targets, identified by ChIP-seq in mouse pre-B cells and Tregs (Ochiai et al., 2012; Ouyang et al., 2012; Webb et al., 2016), with genes downregulated in FOXO1 KO versus WT mouse CD8$^+$ CTLs (1.3-fold and padj <0.05 thresholds applied) (Spinelli et al., 2021). AKT^{BOE}_UP and AKT^{BOE}_DOWN gene sets contain genes upregulated or downregulated in AKT^{BOE} B cells compared with control FO B cells, respectively (Cox et al., 2023). MZ_UP and FO_UP gene sets comprise genes upregulated or downregulated, respectively, in WT MZ compared with WT FO CD45.2$^+$ B cells, determined in the current study (1.5-fold change, padj <0.05). Differential gene expression results and custom gene sets are available in Table S2. RNAseq data have been deposited with GEO (accession number GSE300247).

B cell in vitro culture

To generate LPS blasts for AP and immunoprecipitation experiments, spleens were harvested from mice, red blood cells were lysed, and resting B2 cells were isolated by negative depletion using anti-CD43 MicroBeads and LS magnetic columns (Miltenyi Biotec), according to the manufacturer's protocol, in sterile FACS buffer. Purified B cells were then cultured at 1×10^7 cells per well in 6-well plates (353046; Corning Inc.) with 40 µg/ml LPS (L3129; Sigma-Aldrich) in RPMI 1640 media supplemented with 10% heat-inactivated FCS, 100 U/ml penicillin, 100 µg/ml streptomycin, 2 mM L-glutamine, and 50 µM β-mercaptoethanol (10% FCS/RPMI) for 4 days (for BAFFR AP) or 3 days (for TACI immunoprecipitation) at 37°C, 5% CO_2.

For in vitro plasmablast differentiation assays, MZ B cells from the spleens of WT:WT and KO:WT chimeras were isolated

by FACS, using a staining panel excluding antibodies that bind IgM or IgD to avoid BCR activation. Sorted MZ B cells were then cultured at 0.5 × 10^6 cells per well in 96-well plates (353072; Corning Inc.) with 0.5 µg/ml LPS (L3129; Sigma-Aldrich) in 10% FCS/RPMI media for 72 h at 37°C, 5% CO_2.

For in vitro survival assays, resting B2 cells were isolated from the spleens of WT:WT and KO:WT chimeras by negative depletion, then cultured at 0.729 × 10^6 cells per well in 12-well plates (353043; Corning Inc.) with or without 200 ng/ml BAFF (8876-BF-010/CF; R&D Systems) in 10% FCS/RPMI media for 24–48 h at 37°C, 5% CO_2.

BAFF and APRIL in vitro stimulation and cell lysis

Before in vitro stimulation of LPS blasts, cells were washed by centrifugation and rested in 0.5% FCS/RPMI media at 2 × 10^7 cells/ml for 75 min at 37°C. Cells were then stimulated with 200 ng/ml mouse BAFF (8876-BF-010/CF; R&D Systems) or 200 ng/ml mouse APRIL (7907-AP-010/CF; R&D Systems) in 0.5% FCS/RPMI for 15 min at 37°C with 350 rpm shaking. Cells were immediately pelleted at 800 × *g* for 2 min at 4°C, then resuspended in ice-cold lysis buffer (1% IGEPAL CA-630, 50 mM HEPES, 150 mM NaCl, 1 mM EDTA, 1 mM EGTA, 25 mM NaF, 10 mM iodoacetamide, 2.5 mM sodium pyrophosphate, 5 mM β-glycerophosphate, 5 mM sodium orthovanadate, and 1× Protease Inhibitor Cocktail [ab270055; Abcam]; 80 µl per 1 × 10^7 cells), and incubated on ice for 10 min. Lysates were cleared by centrifugation at 16,000 × *g* for 10 min at 4°C.

BAFFR AP

For each AP, fresh, cleared lysates from 8 × 10^8 LPS blasts (*Tnfrsf13c*$^{\text{Twin-Strep-tag/Twin-Strep-tag}}$ or WT) were incubated with 60 µl washed MagStrep type 3 Strep-Tactin XT beads (2-4090-002; IBA Lifesciences) for 20 min at 4°C with rotation. Beads were washed three times with lysis buffer at 4°C with rotation, and then, proteins were released by incubation with biotin elution buffer (100 mM biotin, 200 mM Tris-HCl, 300 mM NaCl, 2 mM EDTA, pH 8) for 10 min, twice, with eluted proteins collected using a DynaMag-2 Magnet (Thermo Fisher Scientific), then snap-frozen.

Nano-liquid chromatography–tandem mass spectrometry analysis

Biotin-eluted AP samples were reduced with 50 mM dithiothreitol (DTT) for 10 min at 95°C, then alkylated with 15 mM iodoacetamide for 20 min at room temperature with shaking in the dark. Proteins were precipitated with 8 volumes 100% acetone overnight at −20°C, followed by centrifugation at 20,000 × *g* for 30 min at 4°C and two washes with ice-cold 80% acetone and centrifugation at 20,000 × *g*. Air-dried protein pellets were resuspended with sonication in digestion buffer (100 mM HEPES, 1 M guanidine-HCl, pH 8), then incubated with 500 ng LysC for 3 h at 37°C with shaking followed by overnight digestion with 500 ng trypsin at 37°C with shaking, then quenched with 10% TFA to pH 2-3. Peptide samples were analyzed by nano-liquid chromatography–tandem mass spectrometry using an EvoSep One interfaced via a nano-electrospray ion source onto Orbitrap Fusion Lumos Tribrid Mass Spectrometer (Thermo Fisher Scientific). Peptides were separated using the standardized 30 samples per day preformed gradient method. Eluted peptides were ionized by applying a 2.2 kV voltage and introduced to the mass spectrometer as gas-phase ions. MS1 scans were acquired in the Orbitrap mass analyzer with a target of 4 ×10^5 ions or 50-ms maximum injection time, a mass resolution of 60,000, and a scan range of m/z 375–1,500. Ions with charge 2–5 and intensity ≥10,000 from each MS1 scan were isolated in the quadrupole mass analyzer using a 1.2 m/z window and fragmented using higher energy collisional dissociation with normalized collision energy of 32%. Ions were excluded from reselection for 15 s after fragmentation within a 10 ppm dynamic exclusion window. MS2 spectra were acquired in the ion trap mass analyzer at rapid scan rate with a maximum injection time of 300 ms and AGC target of 1 × 10^4 ions, with the scan range set automatically based on the isolated precursor.

Acquired MS data were processed in MaxQuant version 2.6.5.0, and spectra were searched against the mouse UniProt reference proteome (UP000000589, downloaded 20/08/2021) using the Andromeda search engine. Trypsin/P was set as the specific protease with a maximum of two missed cleavage sites allowed. Mass tolerance was set to 20 pmm for the first search and 4.5 ppm for the main search, with fragment mass tolerances set to 0.5 Da. Carbamidomethylation of cysteine was set as a fixed modification, while oxidation of methionine, diglycine remnant on lysine, and acetylation of the protein N terminus were set as variable modifications. A maximum of five modifications were allowed per peptide, with a minimum peptide length of 7 amino acids. A false discovery rate (FDR) of 1% was used for peptide spectrum matches and protein-level identification, and a minimum of one peptide was required for successful protein identification. Razor peptides were used for label-free quantification (LFQ) and intensity-based absolute quantification, with a minimum ratio count of 2 required. Quantitative MS data were analyzed in Perseus version 1.6.15.0 (Tyanova and Cox, 2018; Tyanova et al., 2016). LFQ intensity values for proteins, excluding contaminants, that were quantified in at least one sample were $\log_2$-transformed, missing values were imputed with a constant below-minimum value, and then, two-tailed Student's *t* tests were performed to compare the mean abundance of each protein in BAFF-stimulated BAFFR APs (n = 3) with its mean abundance in control APs (from WT cells; n = 3) or unstimulated BAFFR APs (n = 3). Specific interactors were determined as proteins with a ≥ twofold enrichment in BAFFR APs compared with control APs and a P value ≤0.05. Generated P values were also corrected for multiple hypothesis testing using the permutation-based FDR method in Perseus, with a threshold of 0.20 to generate q values. Full *t* test results and q values can be found in Table S1. Proteomics data have been deposited to the ProteomeXchange Consortium (http://proteomecentral.proteomexchange.org) via the PRIDE partner repository (Perez-Riverol et al., 2019) with the dataset identifier PXD065033.

Phosphoflow

Spleens were harvested from chimeras, red blood cells were lysed, and B2 cells were isolated by negative depletion using

anti-CD43 MicroBeads and LS magnetic columns (Miltenyi Biotec), according to the manufacturer's protocol. B cells were rested in 0.5% FCS/RPMI 1640 media at 4 × 10^6 cells/ml for 75 min at 37°C, with 200 nM idelalisib (7631; R&D Systems) for PI3Kδ-inhibited samples or 10 nM rapamycin (553210; Sigma-Aldrich) for mTORC1-inhibited samples. Cells were stained with anti-CD93 for 30 min on ice, washed, then incubated in 0.5% FCS/RPMI at 2 × 10^7 cells/ml for 5 or 15 min at 37°C with shaking, with idelalisib or rapamycin for inhibited control samples. Cells were fixed by the addition of prewarmed Cytofix buffer for 10 min at 37°C. Fixed cells were stained with anti-CD19 and anti-IgM for 30 min at 4°C, permeabilized with prechilled Perm Buffer III (558050; BD Biosciences) for 30 min on ice, then stained with anti-TACI, anti-CD45.1, anti-CD45.2, anti-IgD, anti-B220, anti-CD1d, and anti-CD21 for 30 min at 4°C. Cells were incubated with anti-p-S6-S235/236 or rabbit IgG isotype control (9865, 8760; Cell Signaling Technology; 0.13 µg/ml) for 30 min at 4°C, or with anti-p-AKT-T308 or rabbit IgG isotype control (48646, 2985; Cell Signaling Technology; 0.25 µg/ml) and anti-p-AKT-S473 or mouse IgG1κ isotype control (562465, 562292; BD Biosciences; 0.12 µg/ml) overnight at 4°C. Samples were analyzed in FACS buffer on an Aurora spectral flow cytometer (Cytek).

TACI immunoprecipitation

Fresh, cleared lysates from 2 × 10^7 LPS blasts were incubated with 2 µg goat polyclonal anti-mouse-TACI (AF1041; R&D Systems) or 2 µg normal goat IgG (AB-108-C; R&D Systems) for 1 h at 4°C with rotation, followed by the addition of 20 µl washed protein-G Dynabeads (10003D; Thermo Fisher Scientific) and further incubation for 30 min at 4°C with rotation. Beads were washed three times with lysis buffer at 4°C with rotation, then proteins were eluted by incubation at 95°C for 5 min in 1× NuPAGE LDS sample buffer (Thermo Fisher Scientific) with 40 mM DTT, and beads were removed using a DynaMag-2 Magnet.

Immunoblotting

Cell lysates were denatured and reduced in 1× NuPAGE LDS sample buffer with 40 mM DTT at 70°C for 10 min. Pre-IP lysates (input) equivalent to 1.25 × 10^6 cells and half of each IP were subjected to SDS-PAGE on NuPAGE 4–12% Bis-Tris Gels (Thermo Fisher Scientific) and proteins transferred onto Immobilon-FL PVDF membrane (Millipore) using the XCell SureLock Mini-Cell Electrophoresis System and XCell II Blot Module (Thermo Fisher Scientific) according to the manufacturer's instructions. Membranes were blocked with 5% BSA in TBST (TBS, 0.001% Tween-20) for 1 h at room temperature, then incubated sequentially with primary antibodies: anti-mTOR (4517; Cell Signaling Technology), anti-p110δ (34050; Cell Signaling Technology), anti-p85α (4257; Cell Signaling Technology), anti-TACI (93005; Cell Signaling Technology), anti-MyD88 (4283; Cell Signaling Technology) in 5% BSA-TBST overnight at 4°C. Washed membranes were incubated with goat anti-rabbit IRDye 680RD (925-68071; LI-COR) or goat anti-mouse IRDye 800CW (925-32210; LI-COR) secondary antibodies at 1:10,000 in 5% BSA-TBST for 1 h at room temperature. Washed and dried membranes were imaged using Odyssey CLx Imaging System (LI-COR).

Statistical analysis

Statistical significance was assessed using an unpaired *t* test, two-way ANOVA with Fisher's LSD test, two-way ANOVA with Šídák's multiple comparisons test, or unpaired Welch's *t* test corrected for multiple comparisons using the Holm–Šídák method to generate P values. Statistical analysis of differential gene expression in the RNAseq data was performed using DESeq2, with padj calculated using the Benjamini–Hochberg method. GSEA NES were computed by permutation testing (1,000 permutations), and padj were calculated using the Benjamini–Hochberg multiple testing correction. Proteomic data were analyzed using a two-tailed Student's *t* test corrected for multiple hypothesis testing using the permutation-based FDR method to generate q values. P values, padj, and q values ≤0.05 were considered significant, rejecting the null hypothesis.

Online supplemental material

Fig. S1 shows analysis of the BAFFR interactome and TACI-deficient mice. Fig. S2 shows analysis of mixed chimeras. Fig. S3 shows analysis of plasmablast differentiation, NP-CGG immunization, EdU labeling, and adoptive transfer studies. Fig. S4 shows surface marker expression, RNAseq analysis, and pS6 staining. Table S1 contains mass spectrometric analysis of proteins copurified with BAFFR-Twin-Strep-tag. Table S2 contains analysis of RNAseq of MZ and FO B cells from KO:WT and WT:WT chimeras.

Data availability

RNAseq data have been deposited with GEO (accession number GSE300247). Proteomics data have been deposited to the ProteomeXchange Consortium with the dataset identifier PXD065033. Other data and materials are available by request to the authors.

Acknowledgments

We thank Dinis Calado and Edina Schweighoffer for critical reading of the manuscript. We thank the Biological Research Facility, and the Genomics, Flow Cytometry and Proteomics Science Technology Platforms of the Francis Crick Institute. We thank Vishva Dixit (Genentech) for the TACI-deficient mice. Schematic figures were created in BioRender (Luff, D. [2026] https://BioRender.com/jt6h2uz).

Victor L.J. Tybulewicz was supported by the Francis Crick Institute (CC 2080), which receives its core funding from Cancer Research UK (CC 2080), the UK Medical Research Council (CC 2080), and the Wellcome Trust (CC 2080). Open Access funding provided by The Francis Crick Institute.

Author contributions: Daisy H. Luff: conceptualization, data curation, formal analysis, investigation, methodology, validation, visualization, and writing—original draft, review, and editing. Lesley Vanes: investigation. Stefan Boeing: data curation, formal analysis, software, and visualization. Victor L.J. Tybulewicz: conceptualization, funding acquisition, project administration, supervision, visualization, and writing—original draft, review, and editing.

Disclosures: The authors declare no competing interests exist.

Submitted: 27 June 2025
Revised: 23 February 2026
Accepted: 27 March 2026

References

Aiba, Y., M. Kameyama, T. Yamazaki, T.F. Tedder, and T. Kurosaki. 2008. Regulation of B-cell development by BCAP and CD19 through their binding to phosphoinositide 3-kinase. *Blood*. 111:1497–1503. https://doi.org/10.1182/blood-2007-08-109769

Bailis, W., and W.S. Pear. 2012. Notch and PI3K: How is the road traveled? *Blood*. 120:1349–1350. https://doi.org/10.1182/blood-2012-06-435099

Bossen, C., T.G. Cachero, A. Tardivel, K. Ingold, L. Willen, M. Dobles, M.L. Scott, A. Maquelin, E. Belnoue, C.A. Siegrist, et al. 2008. TACI, unlike BAFF-R, is solely activated by oligomeric BAFF and APRIL to support survival of activated B cells and plasmablasts. *Blood*. 111:1004–1012. https://doi.org/10.1182/blood-2007-09-110874

Calamito, M., M.M. Juntilla, M. Thomas, D.L. Northrup, J. Rathmell, M.J. Birnbaum, G. Koretzky, and D. Allman. 2010. Akt1 and Akt2 promote peripheral B-cell maturation and survival. *Blood*. 115:4043–4050. https://doi.org/10.1182/blood-2009-09-241638

Cancro, M.P. 2004. Peripheral B-cell maturation: The intersection of selection and homeostasis. *Immunological Rev*. 197:89–101. https://doi.org/10.1111/j.0105-2896.2004.0099.x

Castello, A., M. Gaya, J. Tucholski, T. Oellerich, K.H. Lu, A. Tafuri, T. Pawson, J. Wienands, M. Engelke, and F.D. Batista. 2013. Nck-mediated recruitment of BCAP to the BCR regulates the PI(3)K-Akt pathway in B cells. *Nat. Immunol.* 14:966–975. https://doi.org/10.1038/ni.2685

Castrillon, C., L. Simoni, T. van den Broek, C. van der Poel, E.H. Akama-Garren, M. Ma, and M.C. Carroll. 2023. Complex subsets but redundant clonality after B cells egress from spontaneous germinal centers. *Elife*. 12:e81012. https://doi.org/10.7554/eLife.81012

Chen, J., J.J. Limon, C. Blanc, S.L. Peng, and D.A. Fruman. 2010. Foxo1 regulates marginal zone B-cell development. *Eur. J. Immunol.* 40:1890–1896. https://doi.org/10.1002/eji.200939817

Cinamon, G., M.A. Zachariah, O.M. Lam, F.W. Foss Jr, and J.G. Cyster. 2008. Follicular shuttling of marginal zone B cells facilitates antigen transport. *Nat. Immunol.* 9:54–62. https://doi.org/10.1038/ni1542

Cox, E.M., M. El-Behi, S. Ries, J.F. Vogt, V. Kohlhaas, T. Michna, B. Manfroi, M. Al-Maarri, F. Wanke, B. Tirosh, et al. 2023. AKT activity orchestrates marginal zone B cell development in mice and humans. *Cell Rep.* 42:112378. https://doi.org/10.1016/j.celrep.2023.112378

Descatoire, M., S. Weller, S. Irtan, S. Sarnacki, J. Feuillard, S. Storck, A. Guiochon-Mantel, J. Bouligand, A. Morali, J. Cohen, et al. 2014. Identification of a human splenic marginal zone B cell precursor with NOTCH2-dependent differentiation properties. *J. Exp. Med.* 211:987–1000. https://doi.org/10.1084/jem.20132203

Dominguez-Sola, D., J. Kung, A.B. Holmes, V.A. Wells, T. Mo, K. Basso, and R. Dalla-Favera. 2015. The FOXO1 transcription factor instructs the germinal center dark zone program. *Immunity*. 43:1064–1074. https://doi.org/10.1016/j.immuni.2015.10.015

Eslami, M., S. Schuepbach-Mallepell, D. Diana, L. Willen, C. Kowalczyk-Quintas, C. Desponds, B. Peter, M. Vigolo, F. Renevey, O. Donze, et al. 2024. Unique and redundant roles of mouse BCMA, TACI, BAFF, APRIL, and IL-6 in supporting antibody-producing cells in different tissues. *Proc. Natl. Acad. Sci. USA*. 121:e2404309121. https://doi.org/10.1073/pnas.2404309121

Gardam, S., and R. Brink. 2014. Non-canonical NF-kappaB signaling initiated by BAFF influences B cell biology at multiple junctures. *Front. Immunol.* 4:509. https://doi.org/10.3389/fimmu.2013.00509

Gaudette, B.T., D.D. Jones, A. Bortnick, Y. Argon, and D. Allman. 2020. mTORC1 coordinates an immediate unfolded protein response-related transcriptome in activated B cells preceding antibody secretion. *Nat. Commun.* 11:723. https://doi.org/10.1038/s41467-019-14032-1

Gaudette, B.T., C.J. Roman, T.A. Ochoa, D. Gomez Atria, D.D. Jones, C.W. Siebel, I. Maillard, and D. Allman. 2021. Resting innate-like B cells leverage sustained Notch2/mTORC1 signaling to achieve rapid and mitosis-independent plasma cell differentiation. *J. Clin. Invest.* 131:e151975. https://doi.org/10.1172/JCI151975

Gentle, M.E., A. Rose, L. Bugeon, and M.J. Dallman. 2012. Noncanonical Notch signaling modulates cytokine responses of dendritic cells to inflammatory stimuli. *J. Immunol.* 189:1274–1284. https://doi.org/10.4049/jimmunol.1103102

Grasset, E.K., A. Chorny, S. Casas-Recasens, C. Gutzeit, G. Bongers, I. Thomsen, L. Chen, Z. He, D.B. Matthews, M.A. Oropallo, et al. 2020. Gut T cell-independent IgA responses to commensal bacteria require engagement of the TACI receptor on B cells. *Sci. Immunol.* 5:eaat7117. https://doi.org/10.1126/sciimmunol.aat7117

Gross, J.A., S.R. Dillon, S. Mudri, J. Johnston, A. Littau, R. Roque, M. Rixon, O. Schou, K.P. Foley, H. Haugen, et al. 2001. TACI-Ig neutralizes molecules critical for B cell development and autoimmune disease: Impaired B cell maturation in mice lacking BLyS. *Immunity*. 15:289–302. https://doi.org/10.1016/s1074-7613(01)00183-2

Gross, J.A., J. Johnston, S. Mudri, R. Enselman, S.R. Dillon, K. Madden, W. Xu, J. Parrish-Novak, D. Foster, C. Lofton-Day, et al. 2000. TACI and BCMA are receptors for a TNF homologue implicated in B-cell autoimmune disease. *Nature*. 404:995–999. https://doi.org/10.1038/35010115

Hampel, F., S. Ehrenberg, C. Hojer, A. Draeseke, G. Marschall-Schroter, R. Kuhn, B. Mack, O. Gires, C.J. Vahl, M. Schmidt-Supprian, et al. 2011. CD19-independent instruction of murine marginal zone B-cell development by constitutive Notch2 signaling. *Blood*. 118:6321–6331. https://doi.org/10.1182/blood-2010-12-325944

Hardy, R.R. 2006. B-1 B cell development. *J. Immunol.* 177:2749–2754. https://doi.org/10.4049/jimmunol.177.5.2749

Hardy, R.R., and K. Hayakawa. 2001. B cell development pathways. *Annu. Rev. Immunol.* 19:595–621. https://doi.org/10.1146/annurev.immunol.19.1.595

Hart, G.T., X. Wang, K.A. Hogquist, and S.C. Jameson. 2011. Kruppel-like factor 2 (KLF2) regulates B-cell reactivity, subset differentiation, and trafficking molecule expression. *Proc. Natl. Acad. Sci. USA*. 108:716–721. https://doi.org/10.1073/pnas.1013168108

He, B., R. Santamaria, W. Xu, M. Cols, K. Chen, I. Puga, M. Shan, H. Xiong, J.B. Bussel, A. Chiu, et al. 2010. The transmembrane activator TACI triggers immunoglobulin class switching by activating B cells through the adaptor MyD88. *Nat. Immunol.* 11:836–845. https://doi.org/10.1038/ni.1914

Hoffmann, F.S., P.H. Kuhn, S.A. Laurent, S.M. Hauck, K. Berer, S.A. Wendlinger, M. Krumbholz, M. Khademi, T. Olsson, M. Dreyling, et al. 2015. The immunoregulator soluble TACI is released by ADAM10 and reflects B cell activation in autoimmunity. *J. Immunol.* 194:542–552. https://doi.org/10.4049/jimmunol.1402070

Jellusova, J., A.V. Miletic, M.H. Cato, W.W. Lin, Y. Hu, G.A. Bishop, M.J. Shlomchik, and R.C. Rickert. 2013. Context-specific BAFF-R signaling by the NF-kappaB and PI3K pathways. *Cell Rep.* 5:1022–1035. https://doi.org/10.1016/j.celrep.2013.10.022

Keppler, S.J., F. Gasparrini, M. Burbage, S. Aggarwal, B. Frederico, R.S. Geha, M. Way, A. Bruckbauer, and F.D. Batista. 2015. Wiskott-Aldrich syndrome interacting protein deficiency uncovers the role of the co-receptor CD19 as a generic hub for PI3 kinase signaling in B cells. *Immunity*. 43:660–673. https://doi.org/10.1016/j.immuni.2015.09.004

Kim, M.V., W. Ouyang, W. Liao, M.Q. Zhang, and M.O. Li. 2013. The transcription factor Foxo1 controls central-memory CD8+ T cell responses to infection. *Immunity*. 39:286–297. https://doi.org/10.1016/j.immuni.2013.07.013

Kometani, K., R. Nakagawa, R. Shinnakasu, T. Kaji, A. Rybouchkin, S. Moriyama, K. Furukawa, H. Koseki, T. Takemori, and T. Kurosaki. 2013. Repression of the transcription factor Bach2 contributes to predisposition of IgG1 memory B cells toward plasma cell differentiation. *Immunity*. 39:136–147. https://doi.org/10.1016/j.immuni.2013.06.011

Korotkevich, G., V. Sukhov, N. Budin, B. Shpak, M.N. Artyomov, and A. Sergushichev. 2021. Fast gene set enrichment analysis. *bioRxiv*. https://doi.org/10.1101/060012 (Preprint posted February 01, 2021).

Kraus, M., M.B. Alimzhanov, N. Rajewsky, and K. Rajewsky. 2004. Survival of resting mature B lymphocytes depends on BCR signaling via the Igalpha/beta heterodimer. *Cell*. 117:787–800. https://doi.org/10.1016/j.cell.2004.05.014

Lam, K.P., R. Kuhn, and K. Rajewsky. 1997. In vivo ablation of surface immunoglobulin on mature B cells by inducible gene targeting results in rapid cell death. *Cell*. 90:1073–1083. https://doi.org/10.1016/s0092-8674(00)80373-6

Lechner, M., T. Engleitner, T. Babushku, M. Schmidt-Supprian, R. Rad, L.J. Strobl, and U. Zimber-Strobl. 2021. Notch2-mediated plasticity between marginal zone and follicular B cells. *Nat. Commun.* 12:1111. https://doi.org/10.1038/s41467-021-21359-1

Li, Y., Y. Tang, J. Liu, X. Meng, Y. Wang, Q. Min, R. Hong, T. Tsubata, K. Hase, and J.Y. Wang. 2022. Glia maturation factor-gamma is involved in S1P-induced marginal zone B-cell chemotaxis and optimal IgM production to type II T-independent antigen. *Int. Immunol.* 34:35–43. https://doi.org/10.1093/intimm/dxab097

Love, M.I., W. Huber, and S. Anders. 2014. Moderated estimation of fold change and dispersion for RNA-seq data with DESeq2. *Genome Biol.* 15: 550. https://doi.org/10.1186/s13059-014-0550-8
Mackay, F., W.A. Figgett, D. Saulep, M. Lepage, and M.L. Hibbs. 2010. B-cell stage and context-dependent requirements for survival signals from BAFF and the B-cell receptor. *Immunol. Rev.* 237:205–225. https://doi.org/10.1111/j.1600-065X.2010.00944.x
Mackay, F., S.A. Woodcock, P. Lawton, C. Ambrose, M. Baetscher, P. Schneider, J. Tschopp, and J.L. Browning. 1999. Mice transgenic for BAFF develop lymphocytic disorders along with autoimmune manifestations. *J. Exp. Med.* 190:1697–1710. https://doi.org/10.1084/jem.190.11.1697
Martin, F., and J.F. Kearney. 2000. Positive selection from newly formed to marginal zone B cells depends on the rate of clonal production, CD19, and btk. *Immunity*. 12:39–49. https://doi.org/10.1016/s1074-7613(00)80157-0
Martin, F., A.M. Oliver, and J.F. Kearney. 2001. Marginal zone and B1 B cells unite in the early response against T-independent blood-borne particulate antigens. *Immunity*. 14:617–629. https://doi.org/10.1016/s1074-7613(01)00129-7
Miller, D.J., and C.E. Hayes. 1991. Phenotypic and genetic characterization of a unique B lymphocyte deficiency in strain A/WySnJ mice. *Eur. J. Immunol.* 21:1123–1130. https://doi.org/10.1002/eji.1830210506
Mombaerts, P., J. Iacomini, R.S. Johnson, K. Herrup, S. Tonegawa, and V.E. Papaioannou. 1992. RAG-1-deficient mice have no mature B and T lymphocytes. *Cell*. 68:869–877. https://doi.org/10.1016/0092-8674(92)90030-g
Noviski, M., C. Tan, J. Huizar, V. Vykunta, J.L. Mueller, and J. Zikherman. 2019. Optimal development of mature B cells requires recognition of endogenous antigens. *J. Immunol.* 203:418–428. https://doi.org/10.4049/jimmunol.1900175
Nutt, S.L., P.D. Hodgkin, D.M. Tarlinton, and L.M. Corcoran. 2015. The generation of antibody-secreting plasma cells. *Nat. Rev. Immunol.* 15: 160–171. https://doi.org/10.1038/nri3795
Ochiai, K., M. Maienschein-Cline, M. Mandal, J.R. Triggs, E. Bertolino, R. Sciammas, A.R. Dinner, M.R. Clark, and H. Singh. 2012. A self-reinforcing regulatory network triggered by limiting IL-7 activates pre-BCR signaling and differentiation. *Nat. Immunol.* 13:300–307. https://doi.org/10.1038/ni.2210
Okada, T., A. Maeda, A. Iwamatsu, K. Gotoh, and T. Kurosaki. 2000. BCAP: The tyrosine kinase substrate that connects B cell receptor to phosphoinositide 3-kinase activation. *Immunity*. 13:817–827. https://doi.org/10.1016/s1074-7613(00)00079-0
Okkenhaug, K., A. Bilancio, G. Farjot, H. Priddle, S. Sancho, E. Peskett, W. Pearce, S.E. Meek, A. Salpekar, M.D. Waterfield, et al. 2002. Impaired B and T cell antigen receptor signaling in p110delta PI 3-kinase mutant mice. *Science*. 297:1031–1034. https://doi.org/10.1126/science.1073560
Otero, D.C., S.A. Omori, and R.C. Rickert. 2001. Cd19-dependent activation of Akt kinase in B-lymphocytes. *J. Biol. Chem.* 276:1474–1478. https://doi.org/10.1074/jbc.M003918200
Ou, X., S. Xu, and K.P. Lam. 2012. Deficiency in TNFRSF13B (TACI) expands T-follicular helper and germinal center B cells via increased ICOS-ligand expression but impairs plasma cell survival. *Proc. Natl. Acad. Sci. USA*. 109:15401–15406. https://doi.org/10.1073/pnas.1200386109
Ouyang, W., W. Liao, C.T. Luo, N. Yin, M. Huse, M.V. Kim, M. Peng, P. Chan, Q. Ma, Y. Mo, et al. 2012. Novel Foxo1-dependent transcriptional programs control T(reg) cell function. *Nature*. 491:554–559. https://doi.org/10.1038/nature11581
Perez-Riverol, Y., A. Csordas, J. Bai, M. Bernal-Llinares, S. Hewapathirana, D.J. Kundu, A. Inuganti, J. Griss, G. Mayer, M. Eisenacher, et al. 2019. The PRIDE database and related tools and resources in 2019: Improving support for quantification data. *Nucleic Acids Res.* 47:D442–D450. https://doi.org/10.1093/nar/gky1106
Pillai, S., and A. Cariappa. 2009. The follicular versus marginal zone B lymphocyte cell fate decision. *Nat. Rev. Immunol.* 9:767–777. https://doi.org/10.1038/nri2656
Rahman, Z.S., and T. Manser. 2004. B cells expressing Bcl-2 and a signaling-impaired BAFF-specific receptor fail to mature and are deficient in the formation of lymphoid follicles and germinal centers. *J. Immunol.* 173: 6179–6188. https://doi.org/10.4049/jimmunol.173.10.6179
Rauch, M., R. Tussiwand, N. Bosco, and A.G. Rolink. 2009. Crucial role for BAFF-BAFF-R signaling in the survival and maintenance of mature B cells. *PLoS One*. 4:e5456. https://doi.org/10.1371/journal.pone.0005456
Saito, T., S. Chiba, M. Ichikawa, A. Kunisato, T. Asai, K. Shimizu, T. Yamaguchi, G. Yamamoto, S. Seo, K. Kumano, et al. 2003. Notch2 is preferentially expressed in mature B cells and indispensable for marginal zone B lineage development. *Immunity*. 18:675–685. https://doi.org/10.1016/s1074-7613(03)00111-0
Sasaki, Y., S. Casola, J.L. Kutok, K. Rajewsky, and M. Schmidt-Supprian. 2004. TNF family member B cell-activating factor (BAFF) receptor-dependent and -independent roles for BAFF in B cell physiology. *J. Immunol.* 173: 2245–2252. https://doi.org/10.4049/jimmunol.173.4.2245
Schiemann, B., J.L. Gommerman, K. Vora, T.G. Cachero, S. Shulga-Morskaya, M. Dobles, E. Frew, and M.L. Scott. 2001. An essential role for BAFF in the normal development of B cells through a BCMA-independent pathway. *Science*. 293:2111–2114. https://doi.org/10.1126/science.1061964
Schneider, P., H. Takatsuka, A. Wilson, F. Mackay, A. Tardivel, S. Lens, T.G. Cachero, D. Finke, F. Beermann, and J. Tschopp. 2001. Maturation of marginal zone and follicular B cells requires B cell activating factor of the tumor necrosis factor family and is independent of B cell maturation antigen. *J. Exp. Med.* 194:1691–1697. https://doi.org/10.1084/jem.194.11.1691
Schweighoffer, E., and V.L. Tybulewicz. 2018. Signalling for B cell survival. *Curr. Opin. Cell Biol.* 51:8–14. https://doi.org/10.1016/j.ceb.2017.10.002
Schweighoffer, E., L. Vanes, J. Nys, D. Cantrell, S. McCleary, N. Smithers, and V.L. Tybulewicz. 2013. The BAFF receptor transduces survival signals by co-opting the B cell receptor signaling pathway. *Immunity*. 38: 475–488. https://doi.org/10.1016/j.immuni.2012.11.015
Shulga-Morskaya, S., M. Dobles, M.E. Walsh, L.G. Ng, F. MacKay, S.P. Rao, S.L. Kalled, and M.L. Scott. 2004. B cell-activating factor belonging to the TNF family acts through separate receptors to support B cell survival and T cell-independent antibody formation. *J. Immunol.* 173:2331–2341. https://doi.org/10.4049/jimmunol.173.4.2331
Sintes, J., M. Gentile, S. Zhang, Y. Garcia-Carmona, G. Magri, L. Cassis, D. Segura-Garzon, A. Ciociola, E.K. Grasset, S. Bascones, et al. 2017. mTOR intersects antibody-inducing signals from TACI in marginal zone B cells. *Nat. Commun.* 8:1462. https://doi.org/10.1038/s41467-017-01602-4
Siu, J.H.Y., M.J. Pitcher, T.J. Tull, R.L. Velounias, W. Guesdon, L. Montorsi, K.T. Mahbubani, R. Ellis, P. Dhami, K. Todd, et al. 2022. Two subsets of human marginal zone B cells resolved by global analysis of lymphoid tissues and blood. *Sci. Immunol.* 7:eabm9060. https://doi.org/10.1126/sciimmunol.abm9060
Smulski, C.R., and H. Eibel. 2018. BAFF and BAFF-receptor in B cell selection and survival. *Front. Immunol.* 9:2285. https://doi.org/10.3389/fimmu.2018.02285
Spinelli, L., J.M. Marchingo, A. Nomura, M.P. Damasio, and D.A. Cantrell. 2021. Phosphoinositide 3-kinase p110 delta differentially restrains and directs naive versus effector CD8(+) T cell transcriptional programs. *Front. Immunol.* 12:691997. https://doi.org/10.3389/fimmu.2021.691997
Stark, A.K., A. Chandra, K. Chakraborty, R. Alam, V. Carbonaro, J. Clark, S. Sriskantharajah, G. Bradley, A.G. Richter, E. Banham-Hall, et al. 2018. PI3Kdelta hyper-activation promotes development of B cells that exacerbate *Streptococcus pneumoniae* infection in an antibody-independent manner. *Nat. Commun.* 9:3174. https://doi.org/10.1038/s41467-018-05674-8
Tamahara, T., K. Ochiai, A. Muto, Y. Kato, N. Sax, M. Matsumoto, T. Koseki, and K. Igarashi. 2017. The mTOR-Bach2 cascade controls cell cycle and class switch recombination during B cell differentiation. *Mol. Cell Biol.* 37:e00418. https://doi.org/10.1128/MCB.00418-17
Tan, C., M. Noviski, J. Huizar, and J. Zikherman. 2019. Self-reactivity on a spectrum: A sliding scale of peripheral B cell tolerance. *Immunol. Rev.* 292:37–60. https://doi.org/10.1111/imr.12818
Tardivel, A., A. Tinel, S. Lens, Q.G. Steiner, E. Sauberli, A. Wilson, F. Mackay, A.G. Rolink, F. Beermann, J. Tschopp, and P. Schneider. 2004. The anti-apoptotic factor Bcl-2 can functionally substitute for the B cell survival but not for the marginal zone B cell differentiation activity of BAFF. *Eur. J. Immunol.* 34:509–518. https://doi.org/10.1002/eji.200324692
Thompson, J.S., S.A. Bixler, F. Qian, K. Vora, M.L. Scott, T.G. Cachero, C. Hession, P. Schneider, I.D. Sizing, C. Mullen, et al. 2001. BAFF-R, a newly identified TNF receptor that specifically interacts with BAFF. *Science*. 293:2108–2111. https://doi.org/10.1126/science.1061965
Troutman, T.D., W. Hu, S. Fulenchek, T. Yamazaki, T. Kurosaki, J.F. Bazan, and C. Pasare. 2012. Role for B-cell adapter for PI3K (BCAP) as a signaling adapter linking Toll-like receptors (TLRs) to serine/threonine kinases PI3K/Akt. *Proc. Natl. Acad. Sci. USA*. 109:273–278. https://doi.org/10.1073/pnas.1118579109
Tsuji, S., C. Cortesao, R.J. Bram, J.L. Platt, and M. Cascalho. 2011. TACI deficiency impairs sustained Blimp-1 expression in B cells decreasing long-lived plasma cells in the bone marrow. *Blood*. 118:5832–5839. https://doi.org/10.1182/blood-2011-05-353961
Tull, T.J., M.J. Pitcher, W. Guesdon, J.H.Y. Siu, C. Lebrero-Fernandez, Y. Zhao, N. Petrov, S. Heck, R. Ellis, P. Dhami, et al. 2021. Human marginal zone B cell development from early T2 progenitors. *J. Exp. Med.* 218: e20202001. https://doi.org/10.1084/jem.20202001
Turei, D., A. Valdeolivas, L. Gul, N. Palacio-Escat, M. Klein, O. Ivanova, M. Olbei, A. Gabor, F. Theis, D. Modos, et al. 2021. Integrated intra- and

intercellular signaling knowledge for multicellular omics analysis. *Mol. Syst. Biol.* 17:e9923. https://doi.org/10.15252/msb.20209923

Tyanova, S., and J. Cox. 2018. Perseus: A bioinformatics platform for integrative analysis of proteomics data in cancer research. *Methods Mol. Biol.* 1711:133–148. https://doi.org/10.1007/978-1-4939-7493-1_7

Tyanova, S., T. Temu, P. Sinitcyn, A. Carlson, M.Y. Hein, T. Geiger, M. Mann, and J. Cox. 2016. The Perseus computational platform for comprehensive analysis of (prote)omics data. *Nat. Methods*. 13:731–740. https://doi.org/10.1038/nmeth.3901

Varfolomeev, E., F. Kischkel, F. Martin, D. Seshasayee, H. Wang, D. Lawrence, C. Olsson, L. Tom, S. Erickson, D. French, et al. 2004. APRIL-deficient mice have normal immune system development. *Mol. Cell Biol.* 24: 997–1006. https://doi.org/10.1128/MCB.24.3.997-1006.2004

Vergani, S., K.G. Muleta, C. Da Silva, A. Doyle, T.A. Kristiansen, S. Sodini, N. Krausse, G. Montano, K. Kotarsky, J. Nakawesi, et al. 2022. A self-sustaining layer of early-life-origin B cells drives steady-state IgA responses in the adult gut. *Immunity*. 55:1829–1842.e6. https://doi.org/10.1016/j.immuni.2022.08.018

Vigolo, M., M.G. Chambers, L. Willen, D. Chevalley, K. Maskos, A. Lammens, A. Tardivel, D. Das, C. Kowalczyk-Quintas, S. Schuepbach-Mallepell, et al. 2018. A loop region of BAFF controls B cell survival and regulates recognition by different inhibitors. *Nat. Commun.* 9:1199. https://doi.org/10.1038/s41467-018-03323-8

von Bulow, G.U., J.M. van Deursen, and R.J. Bram. 2001. Regulation of the T-independent humoral response by TACI. *Immunity*. 14:573–582. https://doi.org/10.1016/s1074-7613(01)00130-3

Wang, Y., S.R. Brooks, X. Li, A.N. Anzelon, R.C. Rickert, and R.H. Carter. 2002. The physiologic role of CD19 cytoplasmic tyrosines. *Immunity*. 17: 501–514. https://doi.org/10.1016/s1074-7613(02)00426-0

Webb, A.E., A. Kundaje, and A. Brunet. 2016. Characterization of the direct targets of FOXO transcription factors throughout evolution. *Aging Cell*. 15:673–685. https://doi.org/10.1111/acel.12479

Wen, L., J. Brill-Dashoff, S.A. Shinton, M. Asano, R.R. Hardy, and K. Hayakawa. 2005. Evidence of marginal-zone B cell-positive selection in spleen. *Immunity*. 23:297–308. https://doi.org/10.1016/j.immuni.2005.08.007

Yan, M., H. Wang, B. Chan, M. Roose-Girma, S. Erickson, T. Baker, D. Tumas, I.S. Grewal, and V.M. Dixit. 2001. Activation and accumulation of B cells in TACI-deficient mice. *Nat. Immunol.* 2:638–643. https://doi.org/10.1038/89790

Supplemental material

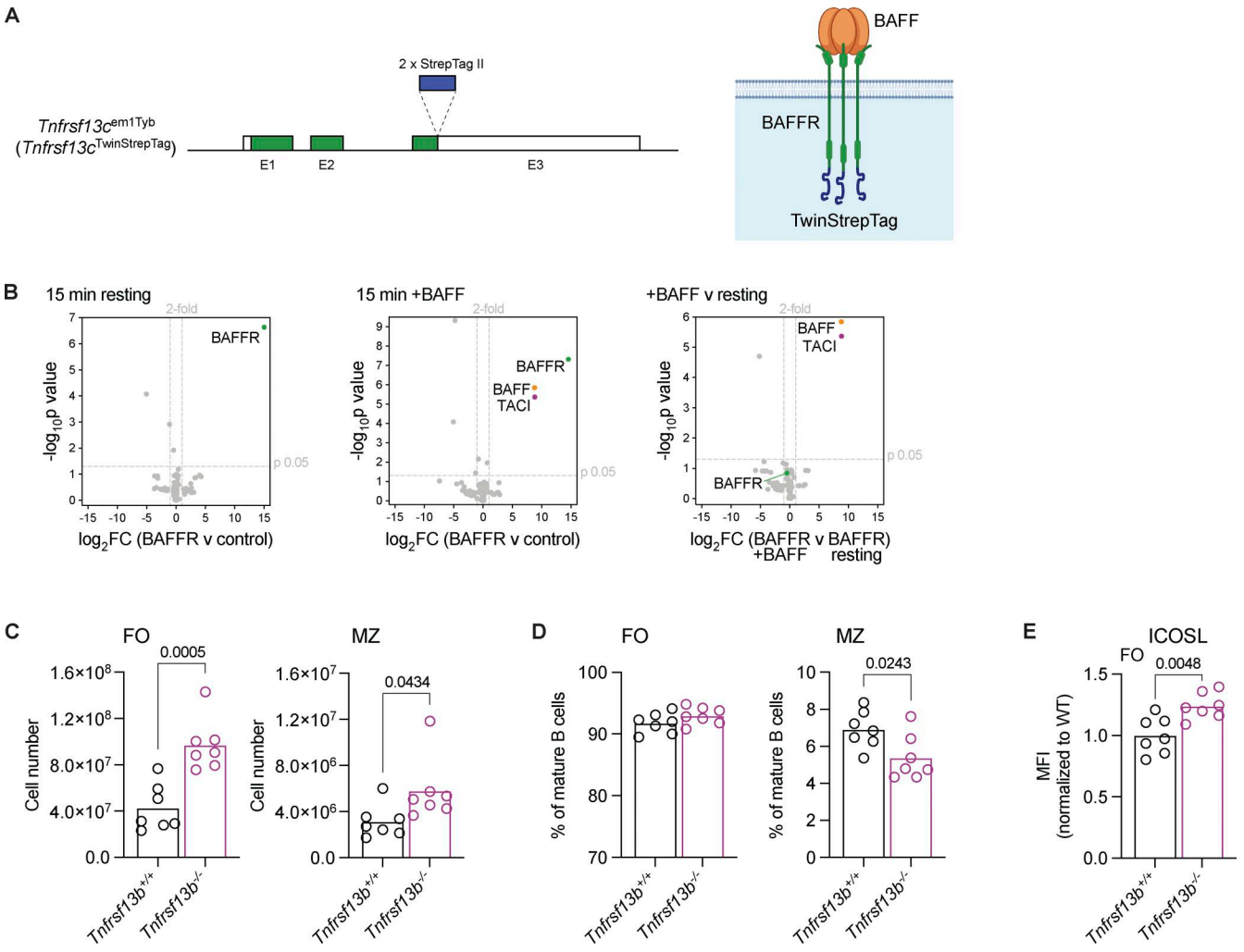

Figure S1. **Analysis of the BAFFR interactome and TACI-deficient mice. (A)** Left, diagram of the *Tnfrsf13c*^{em1Tyb} allele showing exons 1–3 (E1–E3); filled boxes indicate coding sequence; open boxes indicate untranslated regions. Two Strep-tag II sequences were inserted after the last coding codon in E3, before the stop codon. Right, diagram of a BAFFR-Twin-Strep-tag trimer showing the location of the affinity tag at the C terminus of the protein. **(B)** Volcano plots of proteins identified by mass spectrometry in BAFFR-Twin-Strep-tag APs from B cells activated with LPS, either resting or after stimulation with BAFF for 15 min. The plots show the $\log_2$FC in abundance of each protein in BAFFR APs compared with control APs from WT cells ($\log_2$FC(BAFFR v control)) or in stimulated BAFFR APs compared with resting BAFFR APs ($\log_2$FC(BAFFR +BAFF v BAFFR resting)) from three independent experiments, and the $-\log_{10}$p value was determined by two-tailed Student's *t* tests. The thresholds used to determine specific BAFFR interactors (upper right quadrant) are drawn at twofold enrichment and P = 0.05. The full list of proteins identified is in Table S1. **(C and D)** Numbers (C) and proportions (D) of FO (CD1d^{med}IgM^{+}) and MZ (CD1d^{hi}IgM^{hi}) mature splenic B cells (CD93^{-}B220^{+}CD19^{+}) in *Tnfrsf13b*$^{+/+}$ and *Tnfrsf13b*$^{-/-}$ mice. Bars show the mean of *n* = 7 mice, from two independent analyses. Each point represents one mouse. **(E)** ICOSL surface expression, measured by flow cytometry, on splenic FO B cells (CD1d^{med}IgM^{+}CD93^{-}B220^{+}CD19^{+}) from *Tnfrsf13b*$^{+/+}$ and *Tnfrsf13b*$^{-/-}$ mice, quantified as the geometric MFI and normalized to the mean MFI of *Tnfrsf13b*$^{+/+}$ (WT) FO B cells within the same experiment. Bars show the mean of *n* = 7 mice, from two independent analyses. Each point represents one mouse. Statistical tests: unpaired *t* test. Numbers above graphs indicate P values where P ≤ 0.05, otherwise no value is shown. MFI, mean fluorescence intensity; FC, fold change; AP, affinity purification.

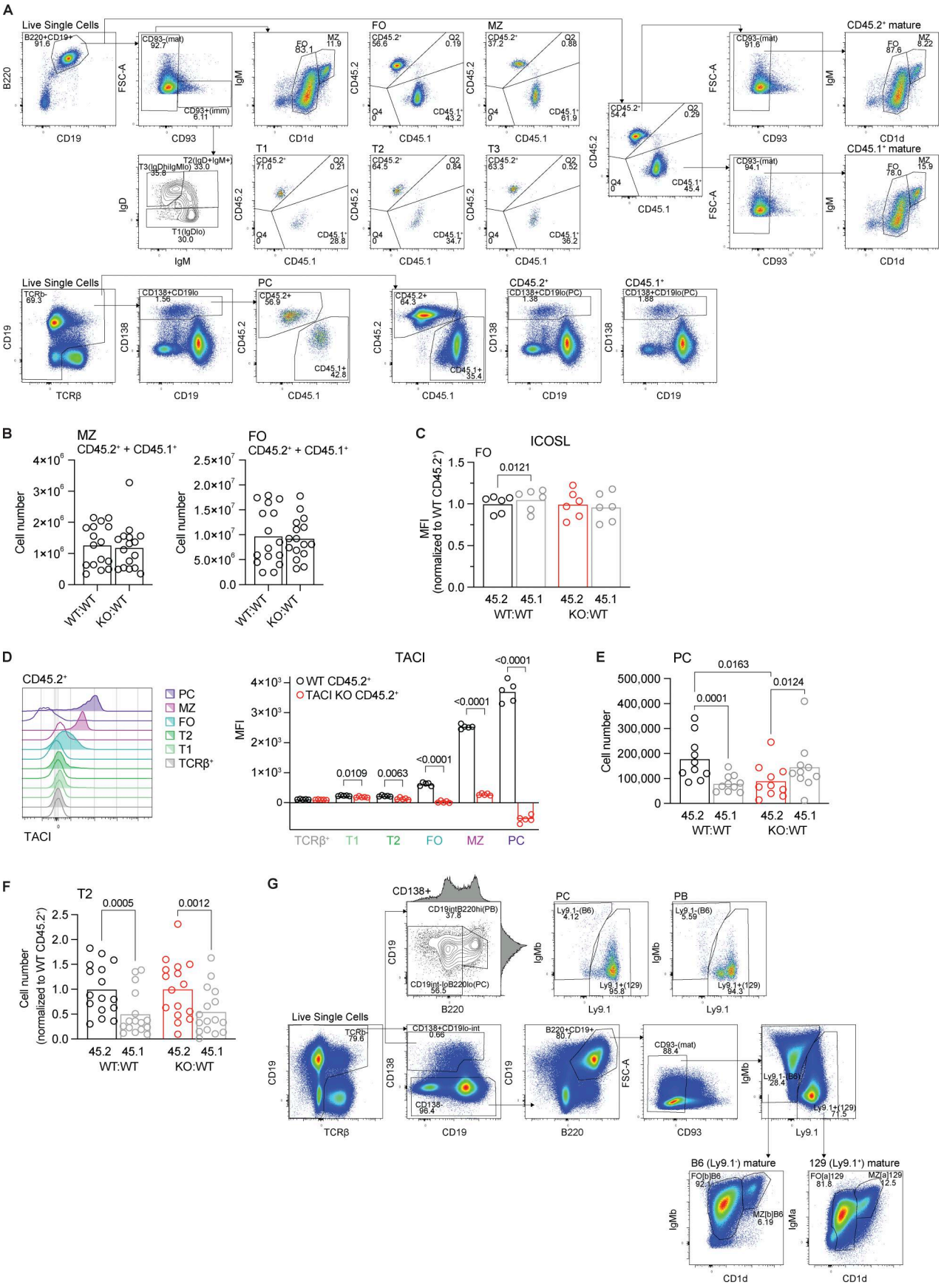

Figure S2. **Analysis of mixed chimeras. (A)** Gating strategy used to identify FO, MZ, T1, T2, and T3 B cells and PCs from the spleens of WT:WT and KO:WT chimeras. **(B)** Total number of MZ ($CD1d^{hi}IgM^{hi}$) and FO ($CD1d^{med}IgM^{+}$) mature splenic B cells ($CD93^{-}B220^{+}CD19^{+}CD138^{-}$; $CD45.2^{+}$ and $CD45.1^{+}$ combined) in WT:WT and KO:WT chimeras. Bars show the mean of *n* = 16 mice, from four independent analyses. Each point represents one mouse. **(C)** ICOSL surface expression, measured by flow cytometry, on $CD45.2^{+}$ and $CD45.1^{+}$ splenic FO B cells ($CD1d^{med}IgM^{+}CD93^{-}B220^{+}CD19^{+}$) from WT:WT and KO:WT chimeras, quantified as the geometric MFI and normalized to the mean MFI of WT $CD45.2^{+}$ cells within the same experiment. Bars show the mean of *n* = 6 mice, from two independent analyses. Each point represents one mouse. Black: WT $CD45.2^{+}$; red: TACI KO $CD45.2^{+}$; gray: WT $CD45.1^{+}$. **(D)** TACI surface expression, measured by flow cytometry, on TACI KO and WT $CD45.2^{+}$ splenic PCs ($TCR\beta^{-}CD138^{+}CD19^{lo}$), MZ ($CD93^{-}CD1d^{hi}IgM^{hi}$), FO ($CD93^{-}CD1d^{med}IgM^{+}$), T2 ($CD93^{+}IgD^{+}IgM^{+}$) and T1 ($CD93^{+}IgD^{lo}$) B cells ($B220^{+}CD19^{+}$), and T cells ($TCR\beta^{+}CD19^{-}$) from WT:WT and KO:WT chimeras. Left: Representative flow cytometry histograms showing TACI expression on each cell type. Filled: WT; unfilled: TACI KO. Right: TACI expression quantified as the geometric MFI. Bars show the mean of *n* = 5 mice, representative of two independent analyses. Each point represents one mouse. Black: WT $CD45.2^{+}$; red: TACI KO $CD45.2^{+}$. **(E)** Numbers of $CD45.2^{+}$ and $CD45.1^{+}$ splenic PCs ($TCR\beta^{-}CD138^{+}CD19^{lo}$) in WT:WT and KO:WT chimeras. Bars show the mean of *n* = 10 mice, from two independent analyses. Each point represents one mouse. Colors are as in C. **(F)** Numbers of $CD45.2^{+}$ and $CD45.1^{+}$ splenic T2 ($CD93^{+}IgD^{+}IgM^{+}$) B cells ($B220^{+}CD19^{+}CD138^{-}$) in WT:WT and KO:WT chimeras. Bars show the mean of *n* = 16 mice, from four independent analyses. Each point represents one mouse. Colors are as in C. **(G)** Gating strategy used to identify B6 ($Ly9.1^{-}$) and 129 ($Ly9.1^{+}$) FO B cells, MZ B cells, PCs ($CD138^{+}B220^{lo}CD19^{int\text{-}lo}$), and PBs ($CD138^{+}B220^{hi}CD19^{int}$) from the spleens of WT:wt and KO:wt chimeras, for the data shown in Fig. 2. Statistical tests: unpaired *t* test (B), repeated-measures two-way ANOVA with Fisher's LSD test (C, E, and F), unpaired Welch's *t* test corrected for multiple comparisons using the Holm–Šídák method (D). Numbers above graphs indicate P values where $P \leq 0.05$, otherwise no value is shown. PCs, plasma cells; PBs, plasmablasts; MFI, mean fluorescence intensity.

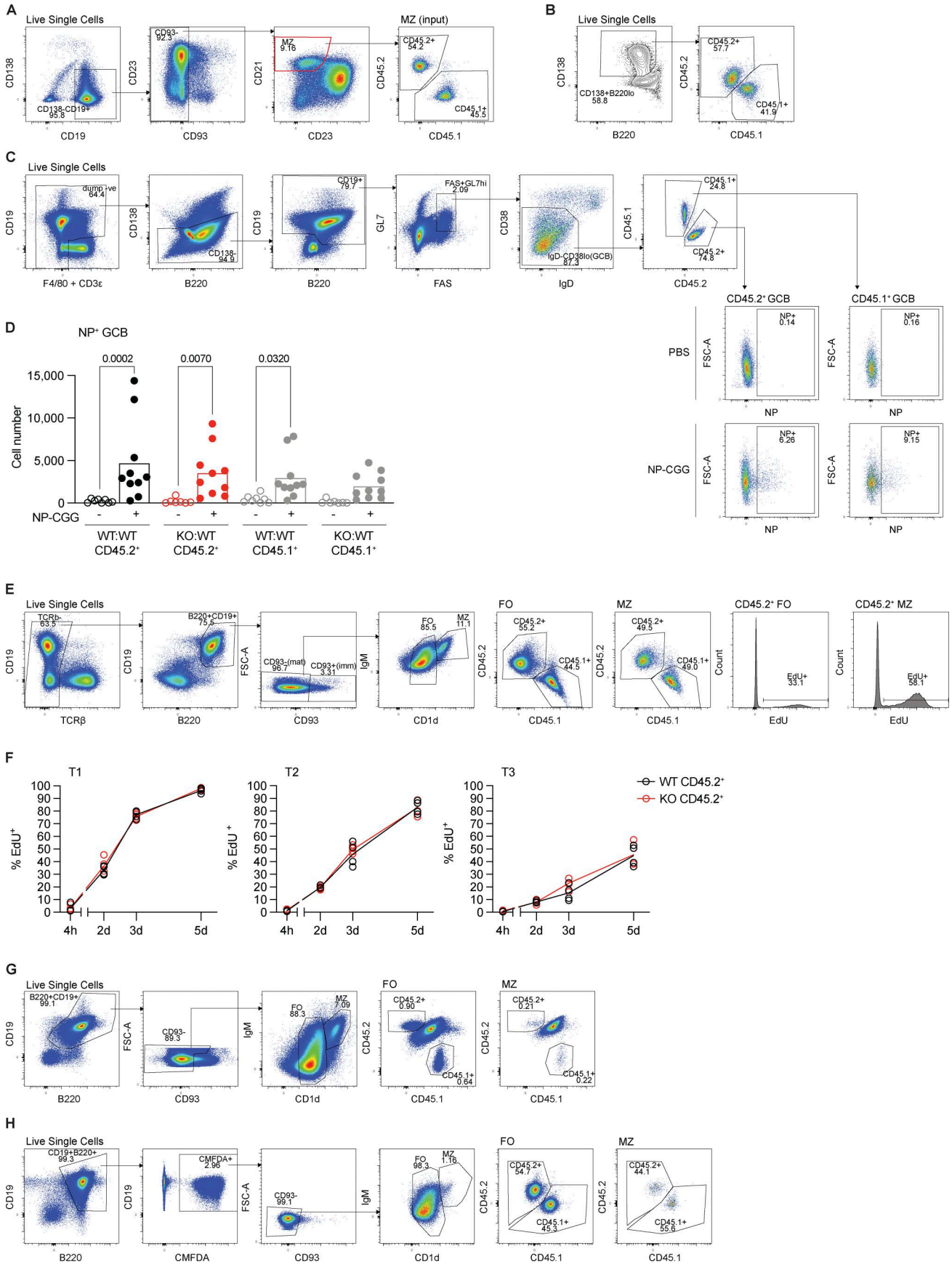

Figure S3. **Analysis of plasmablast differentiation, NP-CGG immunization, EdU labeling, and adoptive transfer studies. (A)** Gating strategy used to purify MZ B cells from the spleens of WT:WT and KO:WT chimeras by FACS for in vitro plasmablast differentiation assays. **(B)** Gating strategy used to identify CD45.2$^+$ and CD45.1$^+$ plasmablasts (CD138$^+$B220^{lo}) after 3 days of in vitro LPS activation of MZ B cells. **(C)** Gating strategy used to identify NP-specific CD45.2$^+$ and CD45.1$^+$ splenic GCBs (CD19$^+$CD138$^-$FAS$^+$GL7^{hi}IgD$^-$CD38^{lo}NP$^+$) 7 days after immunization of WT:WT and KO:WT chimeras with PBS or NP-CGG with alum. **(D)** Numbers of NP-specific CD45.2$^+$ and CD45.1$^+$ splenic GCBs in WT:WT and KO:WT chimeras, 7 days after immunization with PBS or NP-CGG with alum. Bars show the mean of n = 8 (WT:WT +PBS), n = 7 (KO:WT +PBS), or n = 10 (WT:WT and KO:WT +NP-CGG) mice, pooled from two independent experiments. Each point represents one mouse. Black: WT CD45.2$^+$; red: TACI KO CD45.2$^+$; gray: WT CD45.1$^+$. Statistical test: two-way ANOVA with Šídák's multiple comparisons test. Numbers above graphs indicate P values where P ≤ 0.05, otherwise no value is shown. **(E)** Gating strategy used to identify EdU$^+$ CD45.2$^+$ FO and MZ B cells in splenocytes from WT:WT and KO:WT chimeras after continuous EdU labeling in vivo. **(F)** Proportion of EdU$^+$ cells within T1 (IgD^{lo}), T2 (IgD$^+$IgM$^+$), and T3 (IgD^{hi}IgM^{lo}) CD45.2$^+$ immature splenic B cell populations (CD93$^+$B220$^+$CD19$^+$) from WT:WT and KO:WT chimeras at 4 h, and 2, 3, and 5 days after EdU injection (performed at 12 wk after reconstitution) and EdU continuously administered via drinking water. Each point represents one mouse (4 h WT, n = 4; KO n = 5; 2, 3, and 5 days, n = 4). Lines connect the mean at each time point. Black: WT CD45.2$^+$; red: TACI KO CD45.2$^+$. No difference reported between WT and KO means at any time point as determined by two-way ANOVA with Šídák's multiple comparisons test. **(G)** Gating strategy used to identify transferred CD45.2$^+$ and CD45.1$^+$ FO and MZ B cells in the spleens of CD45.2$^+$CD45.1$^+$ recipients, 7 days after adoptive transfer. **(H)** Gating strategy used to identify transferred CMFDA-labeled CD45.2$^+$ and CD45.1$^+$ FO and MZ B cells in the spleens of CD45.2$^+$CD45.1$^+$ recipients, 1 h after adoptive transfer. GCBs, germinal center B cells.

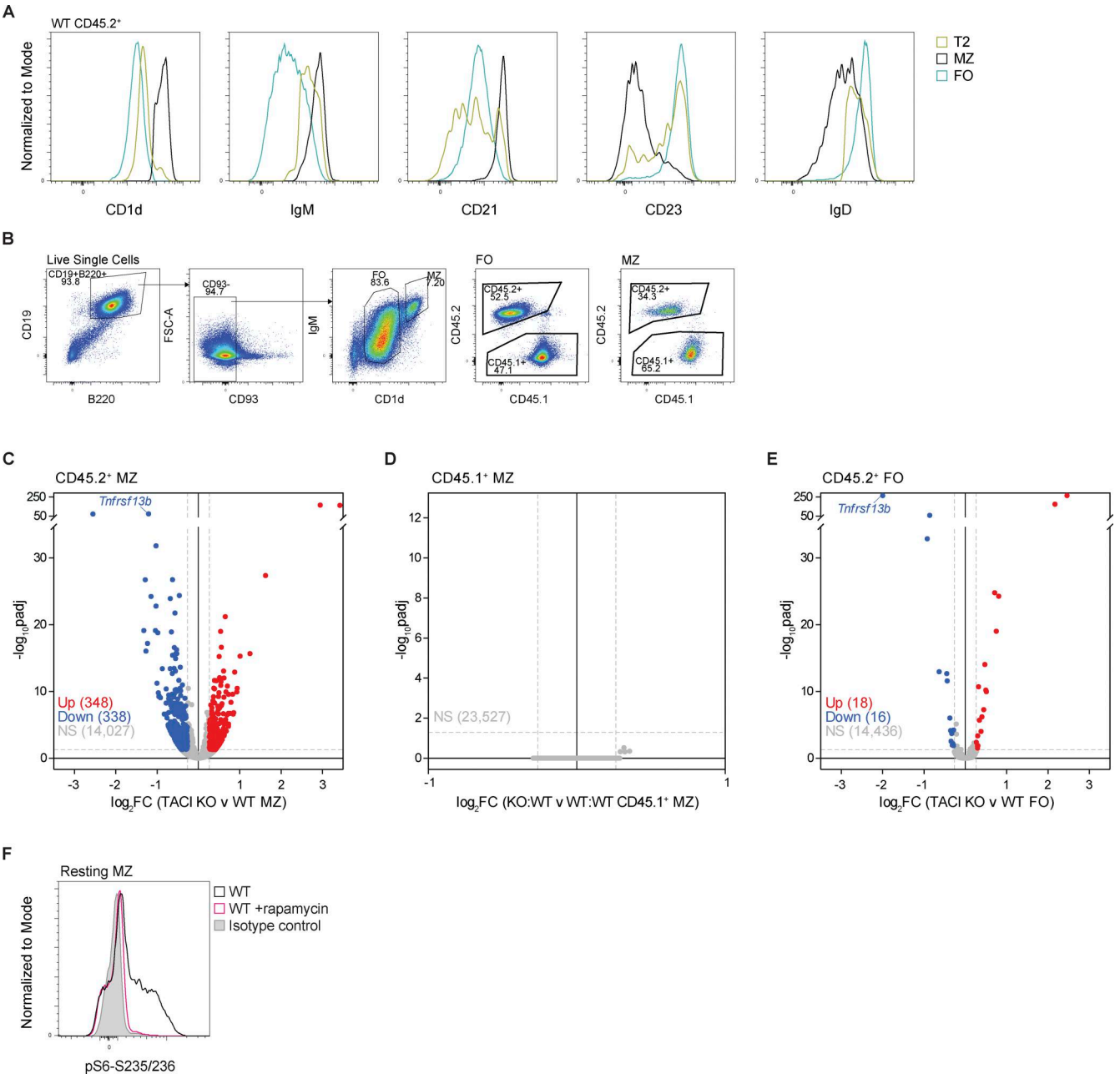

Figure S4. **Surface marker expression, RNAseq analysis, and pS6 staining. (A)** Flow cytometry histograms comparing CD1d, IgM, CD21, CD23, and IgD surface expression on T2 ($IgD^+IgM^+CD93^+$), MZ ($CD1d^{hi}IgM^{hi}CD93^-$), and FO ($CD1d^{med}IgM^+CD93^-$) WT CD45.2+ B cells ($B220^+CD19^+$) from the spleens of WT:WT chimeras. Gold: T2; black: MZ; blue: FO. **(B)** Gating strategy used to sort CD45.2+ and CD45.1+ FO and MZ B cells from the spleens of WT:WT and KO:WT chimeras by FACS for RNAseq. **(C–E)** Volcano plot of differential gene expression between TACI KO and WT CD45.2+ MZ B cells (C), between WT control CD45.1+ MZ B cells from KO:WT and WT:WT chimeras (D), and between TACI KO and WT CD45.2+ FO B cells (E) from KO:WT and WT:WT chimeras, respectively, showing the mean log_2FC and the $-log_{10}padj$ for each gene from $n = 6$ mice. Significantly differentially expressed genes are in red (upregulated; $log_2FC \geq 0.263$, padj <0.05) and blue (downregulated; $log_2FC \leq -0.263$, padj <0.05). Gray: not significantly differentially expressed (NS). Dashed gray lines show the thresholds for 1.2-fold change in gene expression and padj = 0.05. **(F)** Flow cytometry histograms comparing pS6-S235/236 levels in resting WT MZ B cells at 37°C with those treated with the mTORC1 inhibitor rapamycin. Black: WT MZ; pink: WT MZ +10 nM rapamycin; gray: WT MZ cells stained with isotype control antibody. log_2FC, log_2 fold change; padj, adjusted p-value.

Provided online are Table S1 and Table S2. Table S1 shows BAFFR interactome results. Table S2 shows RNAseq differential gene expression analyses and custom gene sets.